QUANTITATIVE PLIF IMAGING IN HIGH-PRESSURE COMBUSTION

Final Technical Report

For the Period

June 11, 1990 to September 20, 1996

Submitted to: NASA – Lewis Research Center
Cleveland, OH

Submitted by: Prof. R.K. Hanson
Mechanical Engineering Department
Stanford University
Stanford, CA 94305

October 13, 1997

HIGH TEMPERATURE GASDYNAMICS LABORATORY
Mechanical Engineering Department
Stanford University
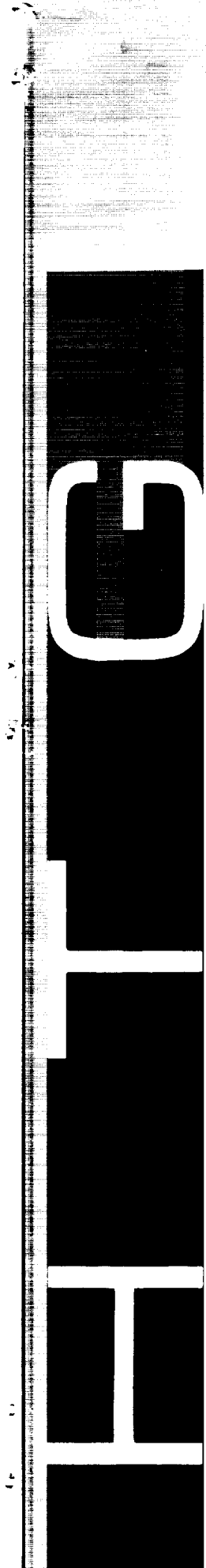
Final Technical Report

On

QUANTITATIVE PLIF IMAGING IN HIGH-PRESSURE COMBUSTION

NASA Grant NAG 3-1185

Prepared for

NASA – Lewis Research Center

Cleveland, OH

For the Period

June 11, 1990 to September 20, 1996

Submitted by

R.K. Hanson, Principal Investigator
Thermosciences Division
Mechanical Engineering Department
Stanford University
Stanford, CA 94305-3032

TABLE OF CONTENTS

1.0 SUMMARY

This is the final report for a research project aimed at developing planar laser-induced fluorescence (PLIF) techniques for quantitative 2-D species imaging in fuel-lean, high-pressure combustion gases, relevant to modern aircraft gas turbine combustors. The program involved both theory and experiment. The theoretical activity led to a spectroscopic models that allow calculation of the laser-induced fluorescence produced in OH, NO and O_2 for arbitrary excitation wavelength, pressure, temperature, gas mixture and laser linewidth. These spectroscopic models incorporate new information on line-broadening, energy transfer and electronic quench rates. Extensive calculations have been made with these models in order to identify optimum excitation strategies, particularly for detecting low levels (ppm) of NO in the presence of large O_2 mole fractions (10% is typical for the fuel-lean combustion of interest). A promising new measurement concept has emerged from these calculations, namely that excitation at specific wavelengths, together with detection of fluorescence in multiple spectral bands, promises to enable simultaneous detection of both NO (at ppm levels) and O_2 or possibly NO, O_2 and temperature. Calculations have been made to evaluate the expected performance of such a diagnostic for a variety of conditions and choices of excitation and detection wavelengths.

The experimental effort began with assembly of a new high-pressure combustor to provide controlled high-temperature and high-pressure combustion products. The non-premixed burner enables access to postflame gases at high temperatures (to 2000K) and high pressures (to 13 atm), and a range of fuel-air equivalence ratios. The chamber also allowed use of a sampling probe, for chemiluminescent detection of NO/NO_2, and thermocouples for measurement of gas temperature. Experiments were conducted to confirm the spectroscopic models for OH, NO and O_2.

2.0 BACKGROUND AND MOTIVATION

This research program was motivated by a critical need for a quantitative, nonintrusive diagnostic method for monitoring nitric oxide (NO) in laboratory studies of advanced low-emissions aircraft combustors. Such measurement capability was regarded as crucial to the evaluation of new, high-pressure combustor designs which were being designed to yield lower NO emissions than previous combustors. The objective of the Stanford research was to investigate the suitability of planar laser-induced fluorescence (PLIF) as a measurement approach, and in particular to establish quantitative methodologies and limits for monitoring low levels of NO at the high-pressure, fuel-lean conditions anticipated for the combustor designs of interest.

While PLIF was relatively mature as a diagnostic method at the time this research program was initiated, having first been demonstrated at Stanford in 1982, nearly all past experience with the method was at near-atmospheric (or lower) pressures. Thus the first phase of our NASA research involved design and assembly of a new combustor, intended to provide a realistic test environment for research on fluorescence spectroscopy of combustion gases at pressures up to 13 atmospheres. The burner is described in Section 3.1 below. Once the burner was operational and calibrated, research was focused on a variety of issues relevant to quantitative fluorescence measurements at high pressures. In particular, attention was given to the influence of laser linewidth, absorption linewidths and shifts, spectral overlap of absorption features, and collisional phenomena including electronic quenching and rotational transfer rates and their dependence on mixture composition, temperature and pressure. Initial work emphasized quantitative fluorescence measurements of OH, owing to the availability of relevant data for the absorption spectrum, line-broadening (and shifts) and quenching rates of OH, and to our ability to make comparative absolute OH measurements by alternate methods. Subsequently, emphasis was placed on extending the OH fluorescence model to O_2 and NO. Although the goal was to monitor NO via fluorescence, our research revealed that the UV absorption and fluorescence spectra of high-pressure (and high-temperature) O_2 and NO overlap strongly, leading to a requirement that detailed spectral models be developed for the absorption and fluorescence spectra of both species.

Following development of detailed spectral models for NO and O_2, we performed high-resolution absorption and fluorescence experiments in the high-pressure burner to improve and validate the computer codes. We then used the codes to explore candidate schemes for quantitative fluorescence measurements of NO. The most important outcome of that research was the development of novel multi-spectral-zone strategies for detection of ppm levels of NO in the presence of a large excess of O_2. With these strategies, a single excitation wavelength is selected, and multiple (two or three) spectral zones of fluorescence are detected. If these spectral channels are properly selected, it appears possible to determine absolute levels of NO, with reasonable independence of temperature and O_2 concentration, or to simultaneously determine NO, O_2 and possibly temperature.

4

3.0   TECHNICAL DISCUSSION   (Note: all figures referred to in Section 3 follow at the end of this section)

In the following sections we provide summary accounts of the primary elements of research conducted in this program, including: fabrication of a high-pressure combustor for spectroscopic studies; development and evaluation of fluorescence spectroscopy models for OH, O_2 and NO; and development of multi-spectral-zone concepts for fluorescence measurements of NO and O_2 at high-pressures and temperatures.

3.1   High-Pressure Combustor

A small-scale combustor was designed and fabricated as a means of providing a spatially uniform and steady sample of combustion gases at known temperatures and pressures. The burner was a non-premixed flat flame burner (Research Technologies, Inc., Pleasanton, CA) incorporating 460 small diffusion flames in a 1-inch square region, surrounded by an outer co-flow (usually nitrogen). The burner was mounted on translation stages (for horizontal and vertical motion) and installed inside a square (4.5 inch x 4.5 inch) containment duct, with windows on four sides for spectroscopic observations. The containment vessel was water cooled, and the static pressure was controlled by choking the flow at the exit of the chamber. Multiple ports were available for thermocouples and sampling probes. Mass flow meters were used for accurate control of fuel, oxidizer and additive compounds. The system was used successfully to 13 atm, with measured postflame temperatures in methane-air (or oxygen) systems to 2200K. Following assembly, an extensive series of tests was run to verify that the burner provided reproducible samples of uniform and steady combustion products, and to calibrate the burner, establish temperature profiles, and measure the concentrations of both OH and NO as a function of height above the burner. Further details of the burner construction and performance may be found in papers 1 and 3 in Section 5.0.

3.2   Fluorescence Spectroscopy of OH

Initial work to develop high-pressure fluorescence models for quantitative species measurements focussed on OH. This species had the benefits of a strong spectroscopic data base and the fact that the postflame levels of OH could be either calculated or measured accurately, thereby providing accurate comparisons with fluorescence-based models and measurements. The basic relation for the laser-induced fluorescence (LIF) signal, in the linear-excitation limit (applicable here) is given by

$$S = C(E/hv)(k\Delta x)\phi$$

where S is the signal, in photons collected per laser pulse, E/hv is the number of incident photons, $k\Delta x$ is the fraction of photons absorbed over the measurement distance Δx, with k the effective spectral absorption coefficient (cm^{-1}), ϕ is the fluorescence yield, i.e. the fraction of absorbed photons which are reemitted as fluorescence, and C is a constant for the optical arrangement which accounts for the efficiency of collecting the fluorescent

5

emission. It is useful to rewrite this result in a form which highlights the influence of pressure,

$$S/\chi_{OH} \propto k' \cdot p \cdot g \cdot \phi$$

where S/χ is the signal per unit mole fraction of the absorbing species, k' is a fundamental quantity known as the line strength (cm^{-2} atm^{-1}) for the transition excited, g is the convolution integral (cm) which combines the effects of the laser lineshape and the molecular absorption lineshape. Details of this development may be found in paper 3 (Section 5.0, reproduced in Section 6.1 of this report).

The quantity k' depends on the temperature and on the excitation transition (or transitions, in the case of overlapping absorption lines) and hence may be taken as known (from existing tabulations or using simple computational codes), and the overlap function is also easily calculated if the laser linewidth (and spectral shape) and absorption linewidth (and shape) are specified, so that the only remaining quantity needed to quantitatively predict the fluorescence signal per unit OH is the fluorescence yield. This is the quantity which normally limits the use of fluorescence for quantitative measurements. Our approach was to calculate the fluorescence yield, using a combination of literature values for collisional quenching cross-sections and reasonable estimates, for a range of postflame pressures, temperatures and combustion gas mixtures (using equivalence as a principal parameter). We then combined these calculations with computed overlap integrals for representative laser linewidths (i.e., typical values for pulsed dye lasers and/or achievable through laser modifications) and absorption lineshapes. For the latter quantity, we utilized the body of absorption line-broadening data for OH collected at Stanford over the past decade, which represents both highly accurate and state-of-the-art data. A typical plot which combines these quantities to indicate the variation of S/χ versus temperature and pressure, for an equivalence ratio of 0.4 (methane-air), a laser linewidth of 1.0 cm^{-1}, and for a specific OH transition, is shown in Fig. 1. Note that the signal does indeed range vary strongly with pressure, as might be expected, but is relatively insensitive to temperature. The results are also not highly sensitive to equivalence ratio in the important fuel-lean regime. The implication of Fig. 1 is that quantitative measurements of OH could be made, without accurate knowledge of temperature, if pressure is known.

The fluorescence model was tested in the high-pressure burner, using a combination of calculated and measured values of OH for comparison. Typical results for single-point LIF measurements of OH are shown in Fig. 2, for pressures between 1.2 and 10.2 atm. The agreement is excellent, thereby providing high confidence in the ability to perform quantitative fluorescence measurements of this species at high pressures. The success of this work (see paper 3) provided a measure of confidence that the same strategy might be usefully employed for the target species NO.

3.3   Fluorescence Spectroscopy of NO and O_2

The primary goal of this research was to establish quantitative PLIF imaging techniques for detection of low levels of NO in high-pressure, fuel-lean combustion

6

products. In order to generate sufficiently strong fluorescence signals for NO, it is necessary to excite the A←X bands (the γ-bands) in the UV, even though it is known that these NO bands overlap the B←X bands of O_2 (Schumann-Runge bands). What was not realized at the initiation of this research program is that the interference problems, while difficult at 1 atm for the relative proportions of O_2 and NO of interest (10,000 to 1 for the case of 10% O_2 and 10 ppm NO) escalate rapidly with increasing pressure. In order to assess this difficulty and to establish optimum excitation-detection strategies, we first compiled detailed spectroscopic models for absorption and fluorescence of the two species, NO and O_2. The absorption models allow calculation of the complete absorption spectra for the bands of interest, subject to specified temperature, pressure, and line-broadening (and line-shift) parameters. These are relatively standard models, in concept, which included the most current data for absorption line positions and strengths, as well as line-broadening and shift parameters which, in the case of NO, were taken from data acquired in our own laboratory under separately funded programs. The fluorescence models are more complex and less common, since they must combine specified excitation wavelengths (and hence depend on laser linewidth and must allow for overlapping collision-broadened absorption lines) with complex fluorescence spectra. The latter depend on specified energy transfer models, e.g. state-dependent rates for rotational, vibrational and electronic transfer, for which little data are available, as well as transition-dependent spontaneous emission rates. Thus, the computation of the emitted fluorescence spectrum, for specified excitation, is both complex and somewhat uncertain, suggesting the need for validation experiments.

The severity of the spectral interference problem is illustrated in Figs. 3 and 4 which present the calculated excitation spectra (assuming broadband fluorescence collection) for O_2 and NO for 2000 K, fuel-lean combustion gases with mole fractions of 10% for O_2 and 10 ppm for NO. Figure 3 provides a broad picture of the interference problem, for P = 10 atm, showing that there are no available spectral regions in which NO can be excited without generating a large signal from O_2. These results suggest that the optimum region for NO excitation is near 226.0 nm, since the relative O_2 to NO signal is smallest here. Figure 4 provides a similar plot, for P = 20 atm, but shown with an expanded scale. These results confirm the severity of the interference problem and also illustrate the critical importance of utilizing detailed codes of this type in the development and evaluation of candidate schemes for quantitative detection of NO at these conditions.

Following completion of the code, experiments were conducted in the high-pressure combustor to evaluate critical elements of the spectroscopic models. These experiments, conducted at pressures up to 12.6 atm and temperatures up to 2200K, involved detailed comparisons of excitation and fluorescence spectra, for both O_2 and NO. Gas mixtures were varied (away from the fuel-lean conditions of Figs. 3 and 4) to allow separation of the spectra of these species; i.e., the fuel-oxidizer mixtures were modified to remove or minimize either NO or O_2. Examples of excitation spectra are given in Figs. 5 and 6, for O_2 and NO respectively. Agreement between the model results and the data were generally very good, though some discrepancies were found, such as that indicated in the region 225.85-225.90 nm in Fig. 5. We attribute this particular difference to the need to include more high-lying rotational transitions (above N = 45) in

7

the absorption spectrum of O_2. Although there are limited or no data for the absolute wavelengths of these high-N transitions, it should be possible to estimate their positions using reasonable extrapolations of the parameters which enter into these calculations, but such changes in the O_2 model have not yet been made.

Similar spectral scans have been made to evaluate the fluorescence codes. Example results for O_2 and NO for specific excitation wavelengths are shown in Figs. 7 and 8. Generally good agreement is found with the O_2 spectra, Fig. 7, though close inspection reveals that under some circumstances the relative positions of overlapping absorption lines may not yet be correct to the level desired. Adjustments of the calculated positions of O_2 lines would, however, require considerable additional experimentation and analysis. The results in Fig. 8 are interesting in that they clearly show the implications of different energy transfer models on the fluorescence spectra of NO. Note that, for these experimental conditions, the observed spectrum falls somewhat closer to the zero-RET (zero rate of rotational energy transfer) model than the full-RET (infinite rate for rotational energy transfer). Data for these rates are not currently available in the literature, though spectra of the type recorded here could be used for that purpose.

Results of the type shown here indicate the status of our computational models for the spectroscopy of NO and O_2. Details of the models and the validation experiments are provided in papers 4-6 listed in Sec. 5.0. For convenience, the key paper, number 6, is reproduced in Sec. 6.2 of this report. In addition, the spectral codes developed in this program, and described in paper 6, may be accessed as described in Sec. 6.3.

3.4   Multi-Spectral-Zone Detection Strategy

The strong spectral interference between the NO and O_2 fluorescence spectra, together with the requirement to detect ppm levels of NO, essentially precludes the usual approach for PLIF, namely the use of a single excitation wavelength and single spectral detection channel. In steady combustion flows, it would be possible to tune the excitation laser and collect multiple broadband fluorescence signals, thereby allowing separation of the contributions of NO and O_2 using a computer model for the excitation spectra of each species. Unfortunately, most of the flows of interest are unsteady, thereby preventing such a strategy. This difficulty led to a new concept, namely the use of a fixed excitation wavelength and separation of the fluorescence signals into multiple-spectral-zones. We used our computational codes to evaluate this strategy, seeking to find an optimum excitation wavelength (and laser linewidth) and optimum spectral collection channels (or zones). Of course there are practical constraints which must be considered, such as the need for sufficient signal level in each zone, the desirability of maximizing the NO signal, the availability and performance of high-efficiency spectral filters, and the need to acquire signals with proper sensitivity (or insensitivity) to variations in temperature and pressure. The value of the code to perform such an optimization, rather than to do this empirically in the laboratory, cannot be overemphasized.

Although it is possible to consider use of more than two zones, we focus here on the performance of a dual-zone-strategy. Shown in Fig. 9 are the fluorescence spectra for

8

one particularly promising selection of spectral zones. The conditions are nominally 10 atm, 2000 K, with fuel-lean combustion products and laser linewidth of 0.5 cm^{-1}. In this example, the NO signal is measured in zone 1 along with an interference from O_2. Zone 2 provides a measure of the O_2 interference signal, which then can be subtracted from the total signal in zone 1. Of course, one can also use the signal in zone 2 by itself as a means of inferring the O_2 concentration. With this dual-zone strategy, it is important that the relative signals of O_2 in zones 1 and 2 be reasonably independent of temperature, as is shown in Fig. 10. In addition, it is desirable for the NO signal to be reasonably independent of temperature, unless an independent measure of temperature is made. As should be clear from Fig. 10, the excitation wavelength and detection channels selected meet our constraints quite well. Other choices for these parameters were evaluated (see paper 6, in Sec. 6.2), but generally with somewhat poorer performance.

Finally, it is important to estimate the probably detection limits of the dual-zone scheme. Toward this objective, we used reasonable estimates of the relevant experimental parameters (particularly laser energy and linewidth and quantities characterizing the optical collection efficiency and conversion to electrical signals), and concluded that it should be possible to detect NO at ppm levels (in the presence of 10% O_2), with acceptable signal-to-noise ratios for all the pressures considered (to 20 atm). Unfortunately, no time remained in the program to evaluate the multi-zone strategy and verify the predicted performance.

It should be noted that there are obvious variations in the multi-zone scheme which may be attractive. For example, there are ways in which three zones could be used for simultaneous imaging of NO, O_2 and temperature. This could be achieved simply by adding a third, temperature-sensitive, channel at short wavelengths (below 220 nm, and hence sensitive to O_2 alone), or by other combinations of spectral channels. We have not conducted further research to broadly evaluate such options or to validate them in the laboratory.

Further details of this work may be found in paper 6.
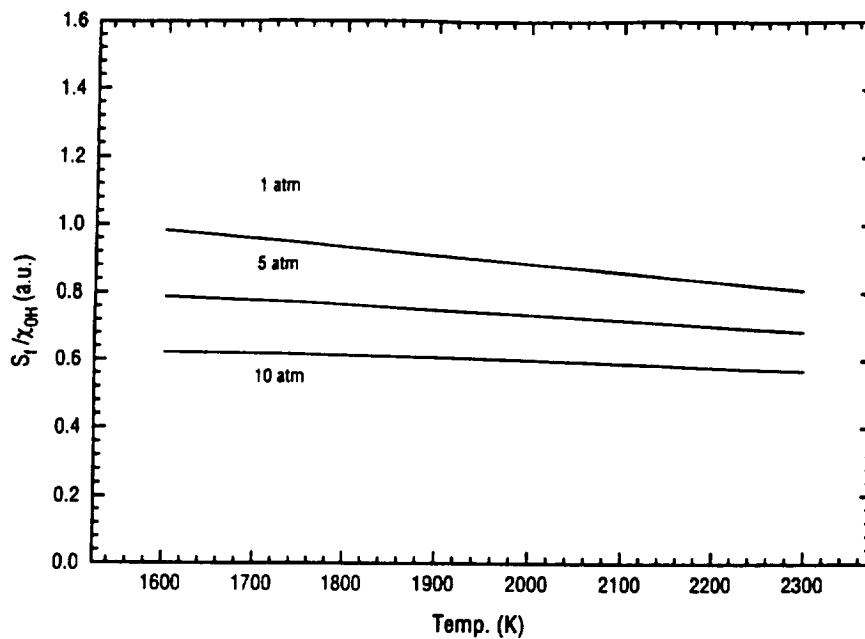
Fig. 1. OH fluorescence signal model as a function of temperature from 1 to 10 atm. Calculations are based on an equivalence ratio of 0.4, the $(1,0)P_1(8)$ transition and a laser bandwith of 1.0 cm^{-1}.
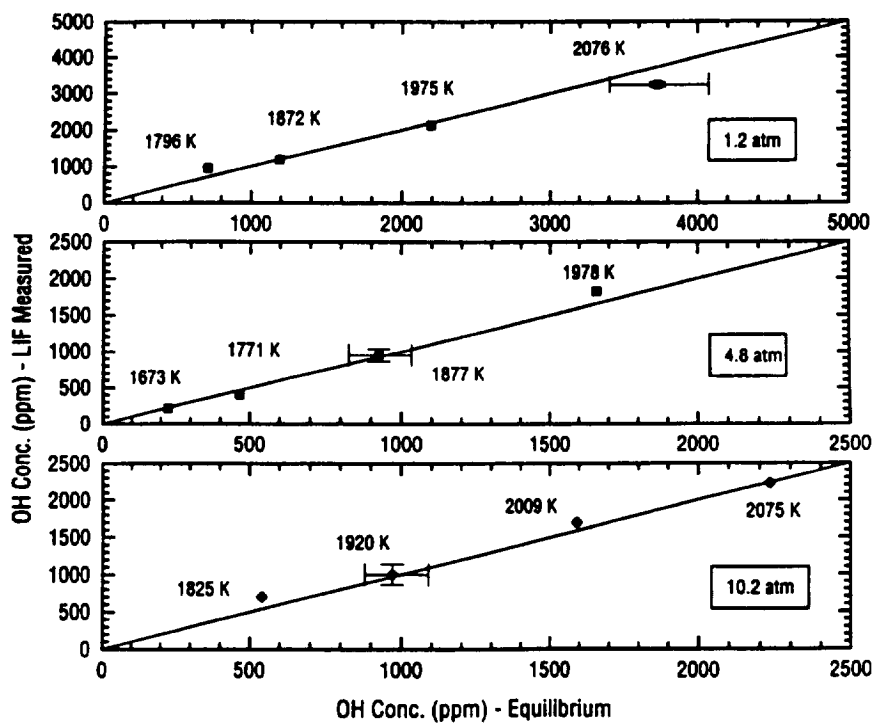
Fig. 2. Single-point model validation results for OH from LIF measurements at 285.685 nm. All data are calibrated at 1.2 atm and 1920 K.
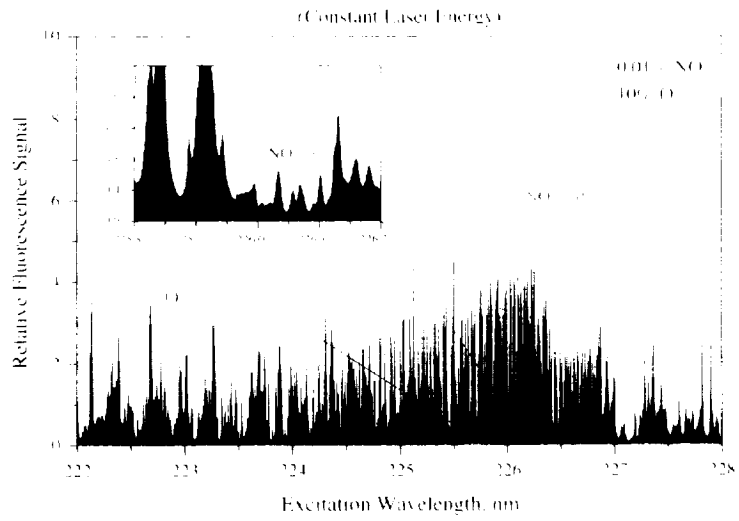
Fig. 3. Calculated broadband fluorescence signals of NO and O_2 for a lean 2000 K, 10 atm CH4/air flame.
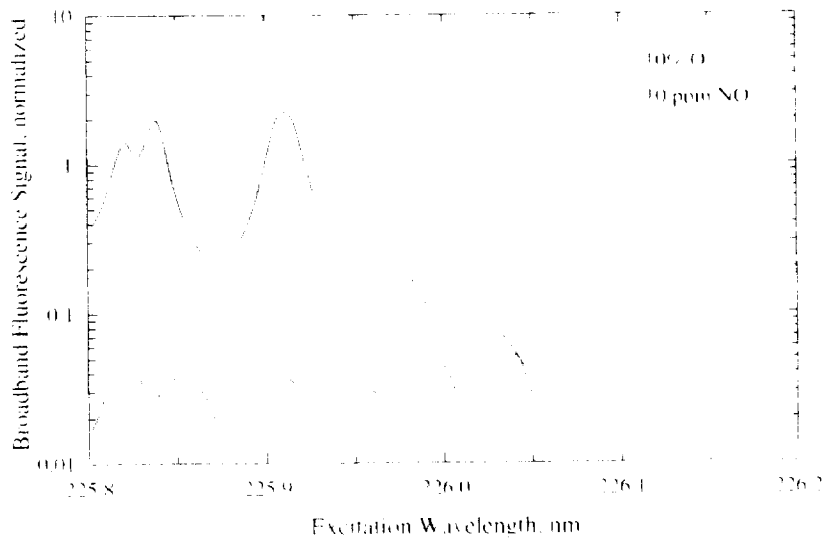
Fig. 4. Excitation spectra of NO $A \leftarrow X$, O_2 $B \leftarrow X$ for 2000 K, 20 atm, 230-290 nm bandpass.

11
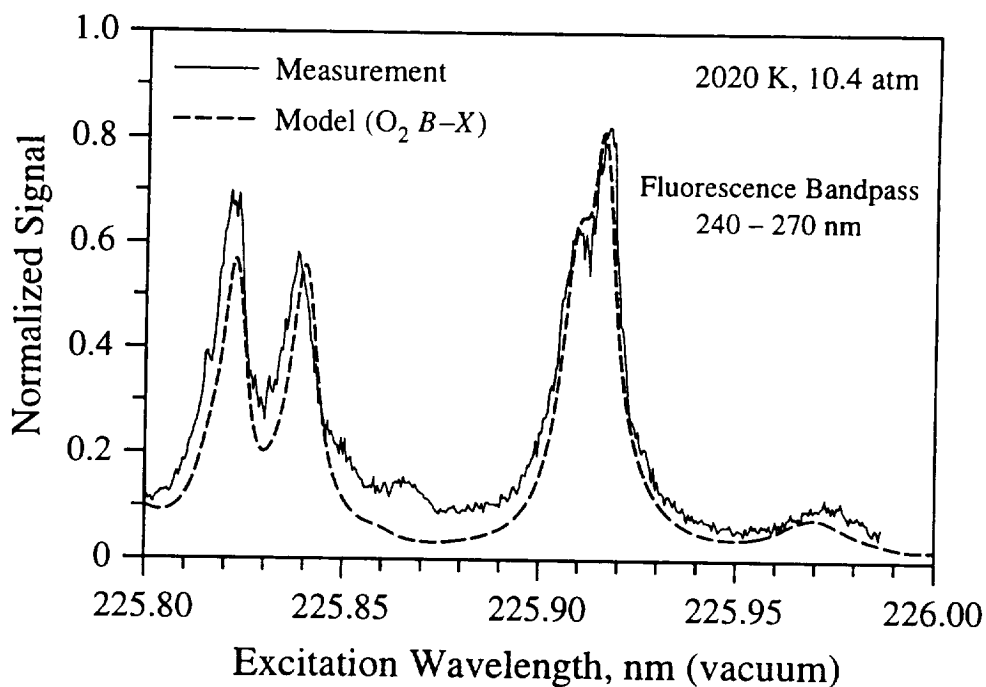
Fig. 5. Measured and modeled excitation spectra of O_2 $B \leftarrow X$ for flame conditions of 2020 K and 10.4 atm, a spectral bandpass from 240-270 nm, and a laser FWHM of 0.5 cm^{-1}.
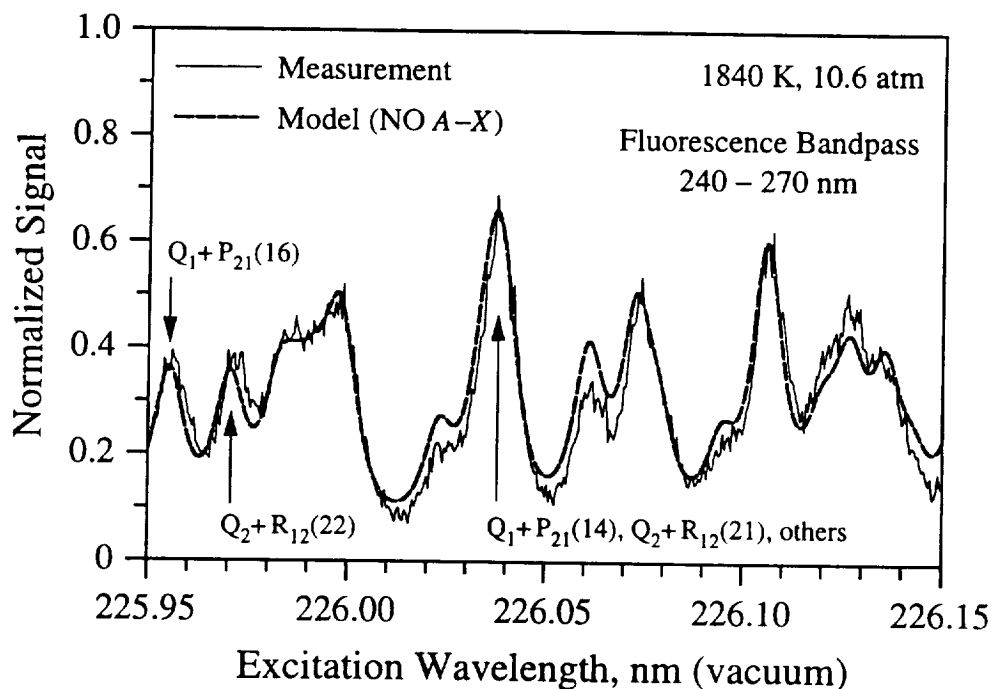
Fig. 6. Measured and modeled excitation spectra of NO $A \leftarrow X$ for flame conditions of 1840 K and 10.6 atm, a spectral bandpass from 240-270 nm, and a laser FWHM of 0.5 cm^{-1}.

12
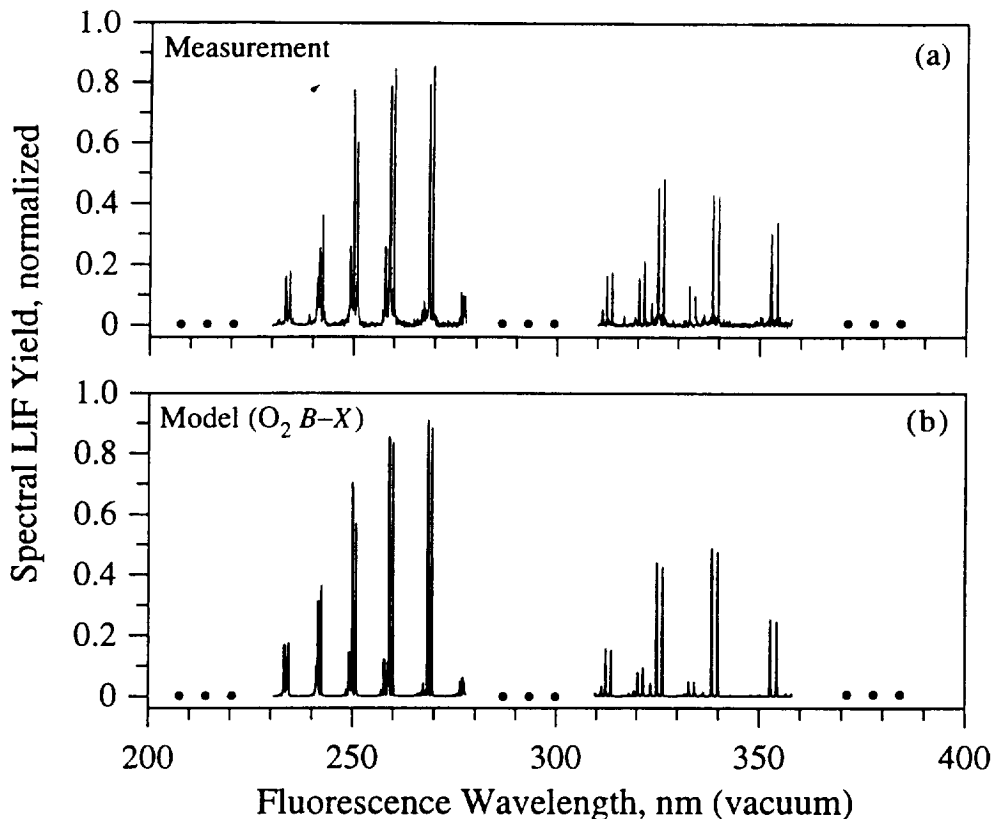
Fig. 7. Fluorescence spectrum of O_2 $B \leftarrow X$ for conditions 2020 K and 10.6 atm as induced by laser excitation at 225.821 nm and of 0.5 cm^{-1} FWHM. (a) measurement. (b) model.
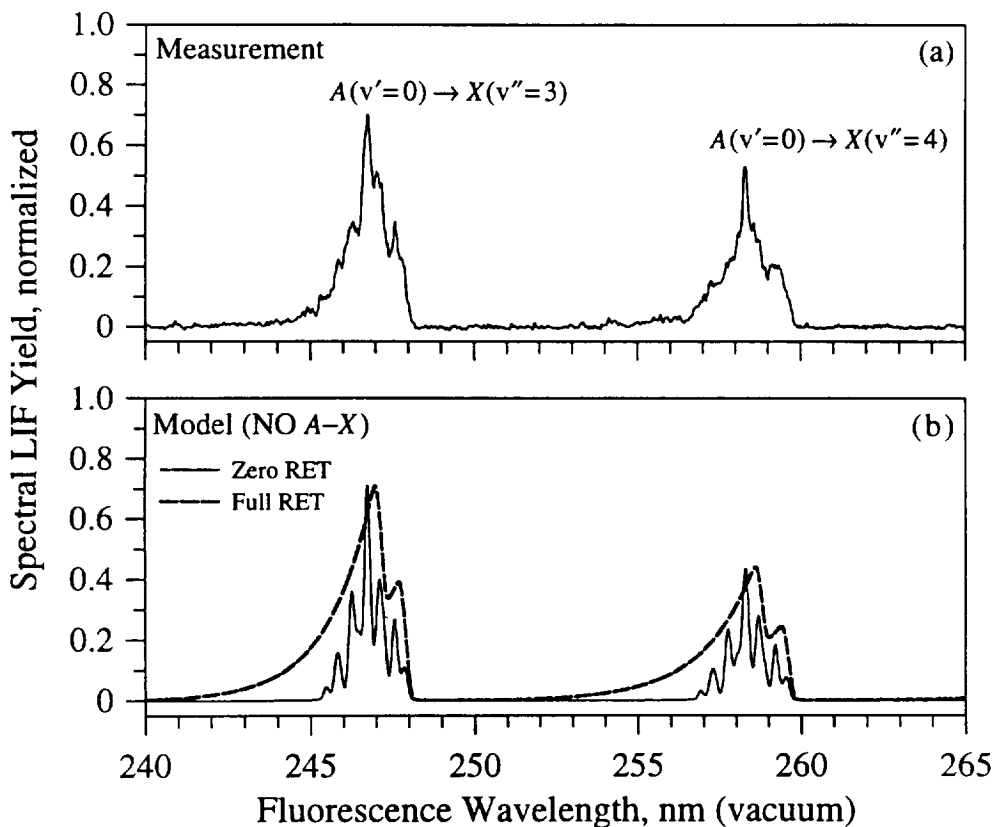
Fig. 8. Fluorescence spectrum of NO $A \leftarrow X$ for conditions 1900 K and 10.6 atm as induced by laser excitation at 226.073 nm and of 0.5 cm^{-1} FWHM. (a) measurement. (b) synthetic spectra for assumptions of zero RET and full rotational equilibrium (full RET) in NO A.

13
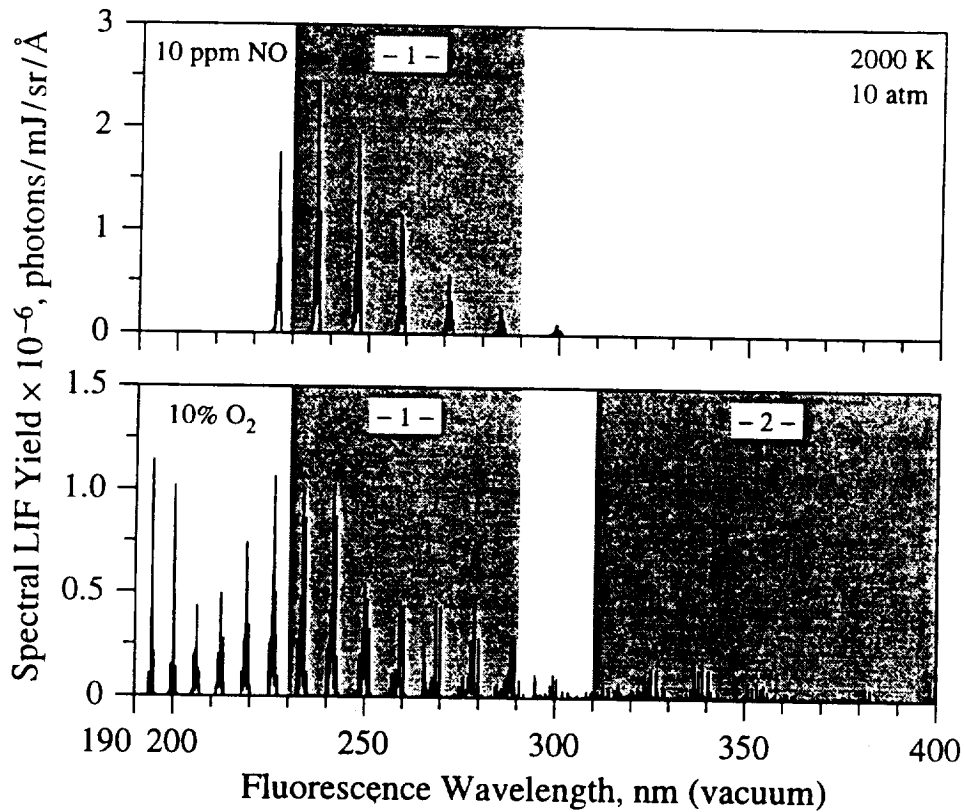
Fig. 9. Calculated fluorescence spectra of NO $A \leftarrow X$ (top panel) and O_2 $B \leftarrow X$ (bottom panel) for an excitaiton wavelength of 226.073 nm, a laser of spectral width 0.5 cm^{-1} FWHM, an ambient gas of major combustion products at 2000 K and 10 atm including 10 ppm NO and 10% O_2, and a FWHM collection bandwith of 1 Å. Widths of shaded areas demarcate zones of fluorescence collection.
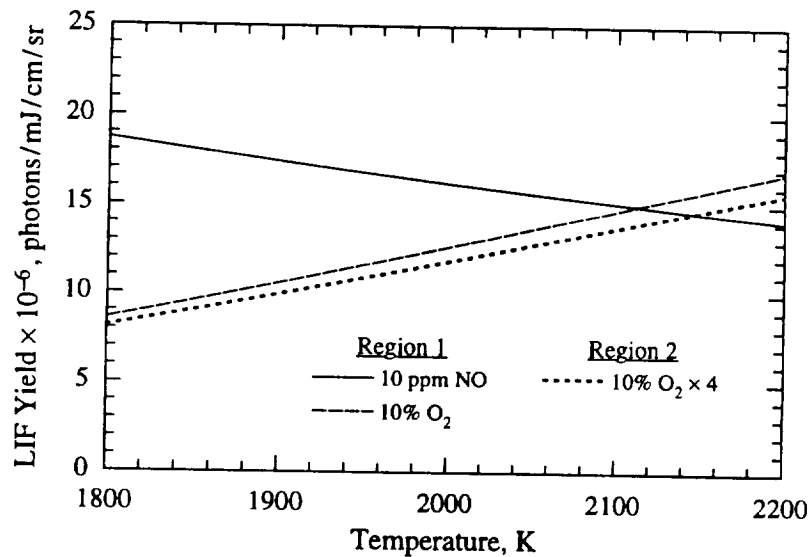
Fig. 10. Temperature variation of the LIF yields of NO and O_2 as spectrally-integrated across regions 1 and 2 shown in Fig. 9. Other than the variable temperature, the gas conditions stated for Fig. 9 apply.

14

4.0   PERSONNEL

This program was supervised by Professor R.K. Hanson. Other participants in the work are listed below.

Research Assistants

Brett Battles (Ph.D. awarded April 1994)

Michael DiRosa (Ph.D. awarded May 1996)

Postdoctoral Research Associates:

Dr. Bradon Yip (1990-1992)

Dr. Jerry Seitzman (1992-1994)

Dr. Kurt Klavuhn (1994-1995)

5.0 PUBLICATIONS AND PRESENTATIONS

Important detail of this research have been recorded in a series of annual progress reports, at review meeting held at NASA Lewis Research Center, in archival publications, and at various meeting in the fields of combustion and laser diagnostics. References to published work are cited below. Papers 3 and 6, which provide detailed accounts of the research approach and key findings are provided in full in Appendices 6.1 and 6.2

1. B.E. Battles and R.K. Hanson, "Laser-Based Measurements of OH in High Pressure CH$_4$/Air Flames," AIAA Paper 91-1494, 22nd Fluid Dynamics, Plasma Dynamics, and Lasers Conference, Honolulu, HI, July 6-9, 1991.

2. B.E. Battles, J.M. Seitzman and R.K. Hanson, "Quantitative Planar Laser-Induced Fluorescence Imaging of Radical Species in High Pressure Flames," AIAA Paper 94-1229, 32nd Aerospace Sciences Meeting, Reno, NV, January 10-13, 1994.

3. B.E. Battles and R. K. Hanson, "Laser-induced Fluorescence Measurements of NO and OH Mole Fraction in Fuel-Lean, High-Pressure (1-10 atm) Methane Flames: Fluorescence Modeling and Experimental Validation," J. Quant. Spectrosc. Radiat. Transfer 54, 521-537 (1995).

4. M.D. DiRosa, K.G. Klavuhn and R.K. Hanson, "PLIF imaging of NO and O$_2$ in High-Pressure Flames," SPIE Proceedings Vol. 2546; presented at SPIE International Symp. on Optical Science, Engineering and Instrumentations, San Diego, CA July 9-14, 1995.

5. M.D. DiRosa, K.G. Klavuhn and R.K. Hanson, "LIF Spectroscopy of NO and O$_2$ in High-Pressure Flames," paper 95F-191 at Western States/Combustion Institute Meeting, Stanford, CA October 30-31, 1995.

6. M.D. DiRosa, K.G. Klavuhn and R.K. Hanson, "LIF Spectroscopy of NO and O$_2$ in High-Pressure Flames," Comb. Sci. and Technol., 118, 257-283 (1996).

LASER-INDUCED FLUORESCENCE MEASUREMENTS OF NO AND OH MOLE FRACTION IN FUEL-LEAN, HIGH-PRESSURE (1–10 atm) METHANE FLAMES: FLUORESCENCE MODELING AND EXPERIMENTAL VALIDATION

BRETT E. BATTLES† and RONALD K. HANSON

High Temperature Gasdynamics Laboratory, Department of Mechanical Engineering,
Stanford University, Stanford, CA 94305–3032, U.S.A.

Abstract—A method for quantifying laser-induced fluorescence (LIF) signals and planar laser-induced fluorescence (PLIF) images of the OH and NO radicals in high pressure flames is presented. The fluorescence signal per unit radical mole fraction is modeled as a function of temperature, pressure, overall flame stoichiometry and laser spectral bandwidth. A recently developed model (*JQSRT*, 51, 511; *Appl. Phys. B*, 57, 249)[1,2] for electronic quenching cross-sections of OH and NO is utilized to express the fluorescence yield as a function of these parameters. The models are confirmed using single-point measurements in the burnt gas region of a flat flame burner at up to 10 atm. The measurements are performed at points in the flame where the temperature, pressure, OH and NO mole fraction are all known. For fuel-lean flames at elevated pressure, interference from the O_2 Schumann–Runge system was found with NO $A \leftarrow X(0, 0)$ fluorescence measurements. This interference must be considered when selecting an appropriate NO transition in this type of environment.

INTRODUCTION

The advent of commercially available lasers has resulted in variety of new spectroscopic techniques of importance to the field of combustion. For example, quantitative measurements of radical and minority species concentrations are essential to the development of accurate flame chemistry models, and non-intrusive, real-time measurement techniques for nitric oxide (NO), a primary pollutant, are crucial in developing prototype low emission propulsion systems. The ubiquity of the hydroxyl radical (OH) in combustion environments has led to its use for marking flame zones, for discerning flow structures, and for determining temperature. The work described herein is motivated by the need for non-intrusive ways to measure the concentrations of these species. Of candidate laser-based methods. laser-induced fluorescence has proven to be a particularly robust and sensitive technique.

Many experimental results can be found in the literature regarding both single-points LIF and PLIF imaging.[1-6] Most prior work on LIF diagnostics has focused on atmospheric or sub-atmospheric pressure application. However, many propulsion devices operate at elevated pressure and this poses unique challenges to fluorescence diagnostics. In particular, quantitative interpretations of linear (i.e., non-saturated) laser-induced fluorescence require accurate accounting of collision-induced phenomena.[7] These phenomena, which include absorption lineshape broadening, radiative trapping and collisional de-activation or quenching, can be severe at elevated pressure. Proper understanding of the fluorescence yield often requires an accurate accounting of the electronic quench rate including species-dependent and temperature-dependent collision cross-sections.

†To whom all correspondences should be addressed. Current address: McKinsey and Co.. 133 Peachtree Street. Suite 2300. Atlanta. GA 30303. U.S.A.

521

The major goals of the work reported here are: (a) to develop straightforward quantitative models of the fluorescence signal, for OH and NO; (b) to investigate the experimental obstacles in making measurements at high pressures; and (c) to confirm the models in 10 atm flat flames.

FLUORESCENCE SIGNAL MODELING

Fluorescence Equation

Laser-induced fluorescence occurs via a multi-step process: absorption to an upper (excited) quantum state, followed by relaxation through either radiative or non-radiative steps, back to the ground state. The fluorescence signal can be modeled by generating the steady-state solution to the population rate equations for the states involved. For a weak non-perturbing laser pulse the total number of fluorescent photons/time striking a photodetector can be expressed as:

$$S_f = C_{ex}\eta_c(k_{v'J'v''J''}\cdot p\chi_{abs})g(\phi_{las};\phi_{abs})\Phi, \qquad (1)$$

where

S_f—fluorescence signal (photons/sec);

C_{ex}—group of experimental constants including laser intensity/area, measurement volume and collection solid angle;

$\eta_c(\lambda)$—transmission efficiency of optical detection system (wavelength dependent);

$k_{v'J'v''J''}$—absorption line strength ($cm^{-2} atm^{-1}$);

p—total pressure (atm);

χ_{abs}—absorbing species mole fraction;

g—overlap of laser lineshape (ϕ_{las}) and molecular absoption lineshape (ϕ_{abs});

Φ—fluorscence yield (the fraction of absorbed photons which are emitted as fluorescence).

Note that this formulation makes no assumptions regarding the relative widths of the laser and absorption spectral lineshapes.

Expressing the fluorescence signal on a per unit absorber mole fraction basis, and removing the experimental constants results in the following proportionality:

$$\frac{S_f}{\chi_{abs}} \propto k_{v'J'v''J''}\cdot pg(\phi_{las};\phi_{abs})\Phi. \qquad (2)$$

Equation (2) also removes η_c, the detection transmission efficiency, for simplicity.

Model Formulation

The goal in modeling the fluorescence signal is to express Eq. (2) in terms of known, or easily measureable global parameters. The parameters chosen for this work are temperature, pressure, laser bandwidth (Δv_{las}) and overall flame equivalence ratio which will be denoted by r. The model can then be validated in flows where these parameters are known or have been previously measured.

Absorption line strength—$k_{v'J'v''J''}$. The absorption line strength represents the intensity of the coupling between the lower and upper quantum states. This term is a function of temperature (through the Boltzmann population fraction) and lower rotational level.[8] As an example, Fig. 1 shows OH line strengths in the $A \leftarrow X(1,0)$ band for several different lower state rotational levels (J'') transitions, as a function of temperature.

Overlap integral (g). The overlap of the laser and absoption lineshapes is included in this formulation of the fluorescence signal so that no assumptions need to be made regarding their relative spectral widths. In high-pressure combustion environments, the molecular absorption linewidths of OH and NO are greater or at least equal to the typical spectral bandwidths of most
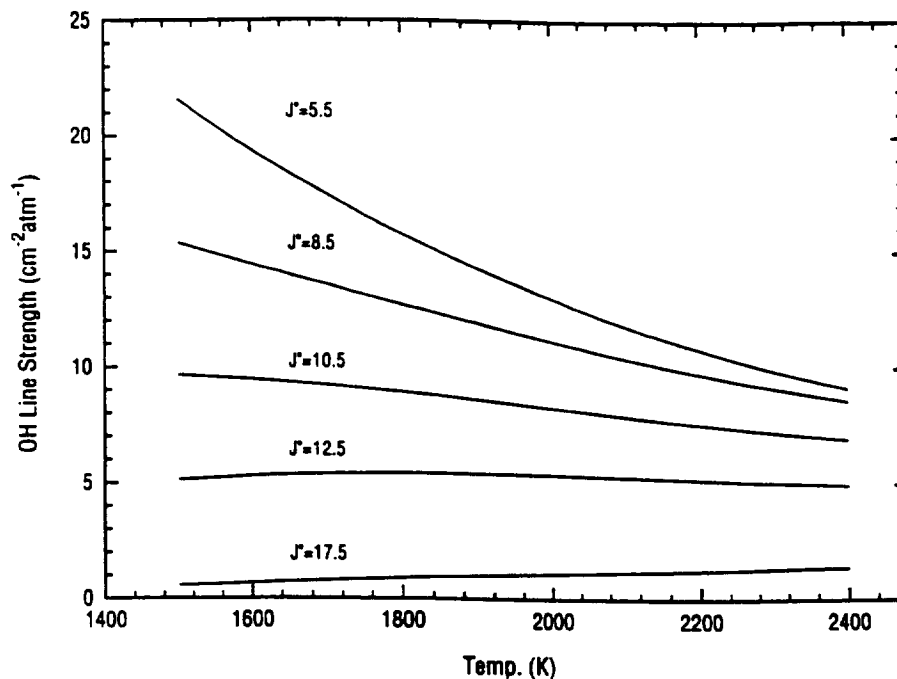
Fig. 1. OH absorption line strength ($k_{v,J',J'}$) shown for various lower rotational levels (J'') as a function of temperature.

commercially available lasers (e.g., $0.5 \, \text{cm}^{-1}$). The overlap term is the product of the laser and absorption lineshapes, integrated over all frequencies:

$$g = \int_{-\infty}^{\infty} \phi_{abs}(v, v_o, \Delta v_{abs}) \cdot \phi_{las}(v, v_o, \Delta v_{las}) \, dv, \quad (3)$$

where v_o is the central frequency and Δv is the spectral FWHM (in cm^{-1}) of either the laser or absorption transition. The laser lineshape (ϕ_{las}) for the work decribed herein is assumed to be
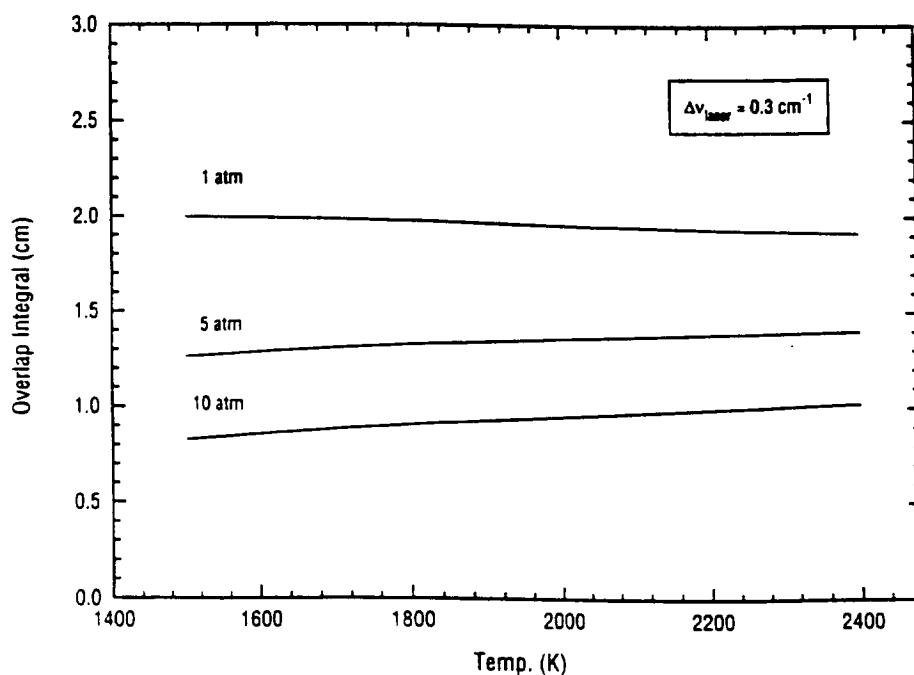
Fig. 2(a). OH overlap integral (g) from 1 to 10 atm as a function fo temperature for a laser bandwidth of $0.3 \, \text{cm}^{-1}$.

Gaussian on average so that the lineshape can readily be calculated based on the laser FWHM and the central frequency. The molecular absorption lineshape. however, is generally a function of temperature, presssure, and composition of the surrounding environment.

Various experimental studies can be found in the literature which express molecular absorption lineshapes as a function of temperature, pressure and rotational level.[9-13] In this work we have used the results given in Ref. 9 for OH lineshape and the results of Ref. 12 for NO lineshape expressions.

Calculated results of the overlap integral are shown in Fig. 2 for OH. The observed trends are also typical for NO albeit the NO linewidths are about twice those of OH. The plots show variations with temperture, pressure, and laser bandwidth. The overlap integral is highly pressure dependent, shown in Fig. 2(a), owing to the pressure broadening of the absorption lineshape. while only slightly temperature dependent. The variation in the overlap integral with laser bandwidth is shown in Fig. 2(b). As indicated, the pressure dependence is reduced when larger bandwidths are used. Large bandwidth lasers also are experimentally more convenient in that they are easier to tune to line center in high-pressure environments and the resulting overlap with the molecule of interest is less sensitive to fluctuations in the laser output wavelength. They do, however, tend to reduce the overall magnitude of the recorded signal. Typical bandwidths of standard commercial Nd:YAG and excimer-pumped dye lasers are on the order of 0.05–0.4 cm^{-1} in the u.v.

Fluorescence yield (Φ)

The fluorescence yield or Stern–Vollmer ration, Φ, represents that fraction of absorbed laser photons which are re-emitted in the form of fluorescence. For a simple two-level system the fluorescence yield is given by:

$$\Phi = \frac{A_{12}}{A_{12} + Q_c} \tag{4}$$

where A_{12} is the Einstein spontaneous emission coefficient and the Q_c is the collisional quench rate. The quench rate can be written as:

$$Q_c = n \sum_i \chi_i \sigma_i v_i, \tag{5}$$
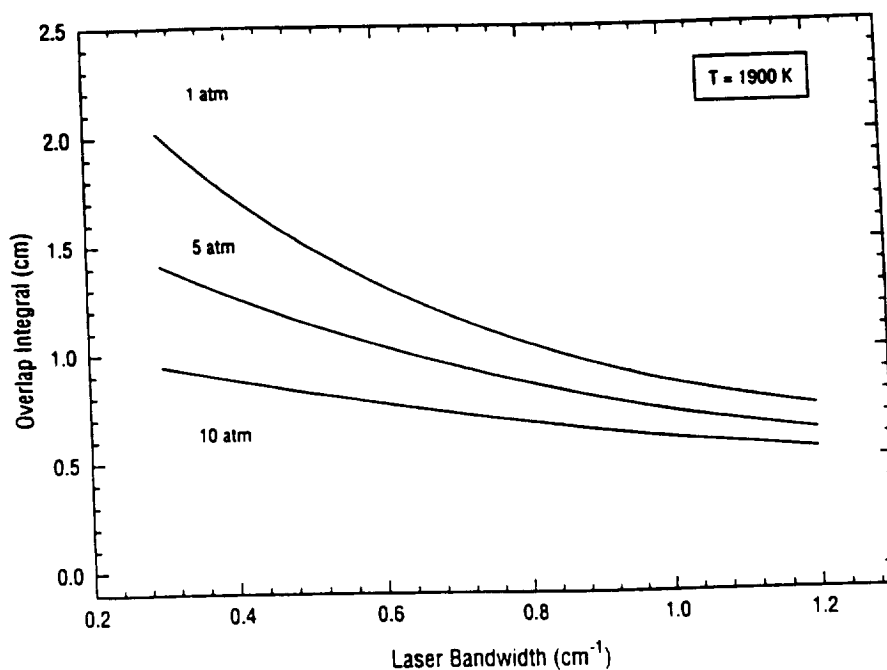
Fig. 2(b). OH overlap integral at 2100 k. 1–10 atm. as a function of laser bandwidth.

where

n—total number density $= p/kT$;
χ_i—collider species mole fraction;
σ_i—collision cross-section;
v_i—mean molecular speed between the absorbing species and colliding species.

The summation is over all i species which can collide and de-excite the absorbing species. While molecules are in reality multi-level systems, this simpler formulation for Φ provides accurate results.

For OH and NO in flame environments at atmospheric (or greater) pressure, Q_c is typically much greater than A_{12}.[14] Furthermore, the Einstein coefficient represents a known constant which can be included in the proportionality expressed in Eq. (2). The fluorescence yield can than be written as:

$$\Phi \propto \frac{1}{\frac{p}{kT}\sum_i \chi_i \sigma_i(T)\left\{\frac{8kT}{\pi\mu_i}\right\}^{0.5}},$$ (6)

where μ_i is the reduced mass of the ith collider.

Colliding species mole fraction. For either OH or NO the identity of the pertinent colliding species must first be established to perform the summation in Eq. (6). Downstream of the flame zone, in the burnt gas region, the product gases consist predominantly of the major combustion product species. For lean hydrocarbon flames, these are CO_2, H_2O, O_2 and N_2.

In lean flames the major product species mole numbers are therefore, mole fractions, can be uniquely specified by the overall flame equivalence ratio, r:

$$rCH_4 + 2(O_2) + qN_2 \rightarrow rCO_2 + 2rH_2O + 2(1-r)O_2 + qN_2,$$ (7)
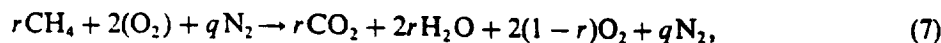
for q moles of N_2 in the reactants. This is shown above for CH_4 but is applicable to any hydrocarbon fuel. This approach constrains the model's applicability to burnt gas regions of lean hydrocarbon flames in favor of experimental and mathematical simplification. However, the same approach is applicable in other regions or flow fields as long as the collider species mole fractions (and cross-sections) are satisfactorily known or can be determined.

Collision cross-sections. Electronic quenching of flame radicals has been extensively studied, particularly for OH. In general, collision cross-sections are species, temperature, and quantum-state dependent. Several reports of OH and NO measurements can be found in the literature for various values of these parameters. Unfortunately, no comprehensive experimental study exists which reports cross-sections at flame temperatures, over a wide range of quantum states and species.

For OH, several detailed studies can be found regarding collisions with H_2O.[15-17] These data are illustrative in that the trends that exist with H_2O are representative of many other collider species. Two trends are evident. First, the rotational level dependence diminishes as the level (J'') increases. Second, the cross-sections tend to be only weakly temperature dependent at elevated temperatures. These trends and data typify the other important collider species: CO_2, O_2 and N_2.

Less experimental data for NO than for OH can be found. However, NO quenching measurements are currently an active area of research due to the importance of measuring NO in a variety of applications. The present experimental evidence indicates that electronic quenching cross-sections for NO are independent of rotational level, at least above room temperature.[18,19] Similar to OH, NO cross-sections also exhibit weak temperature dependencies at elevated temperatures with the exceptions of quenching by N_2.

Analytical models of the quenching cross-sections for OH and NO would be convenient for incorporation into Eq. (6). Models found in the literature[20] typically predict an inverse power law for the cross-section temperature dependence. This type of temperature dependence is in good agreement with experimental results at low temperatures but not so at temperatures likely to be encountered in flame environments.
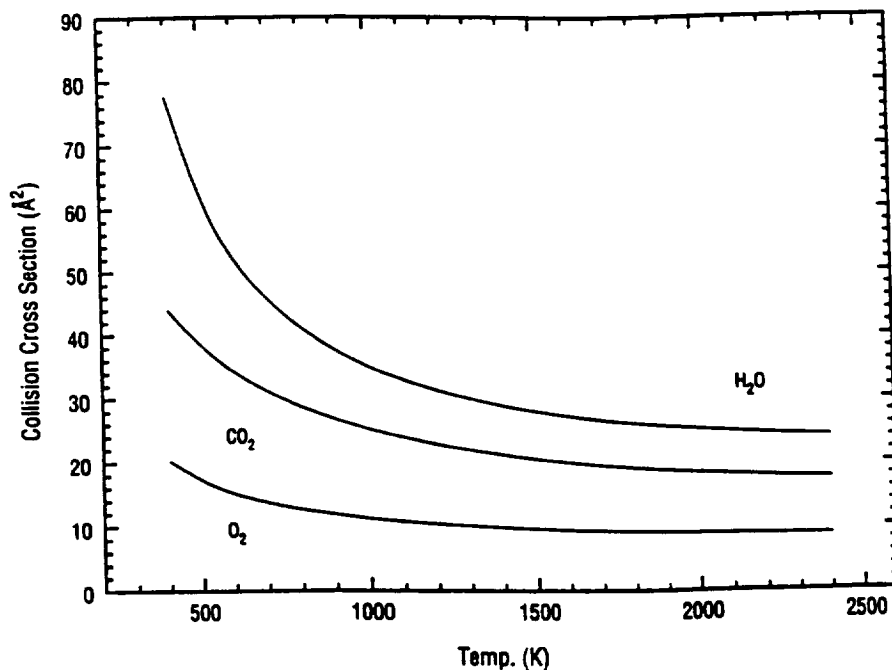
Fig. 3(a). Model calculations of collision cross-sections of various colliders with OH as a function of
temperature.

Recently, however, Paul and co-workers[1,2] have reported the development of models for NO and
OH cross-sections which show good agreement with a wide range of experimental observations.
This model overcomes the main shortcomings of previous models, namely the proper treatment
of cross-section temperature dependence. These treatments are based on the electron transfer or
"harpoon" mechanism and are found to adequately describe the experimentally observed
behaviour of collision quenching of OH and NO.
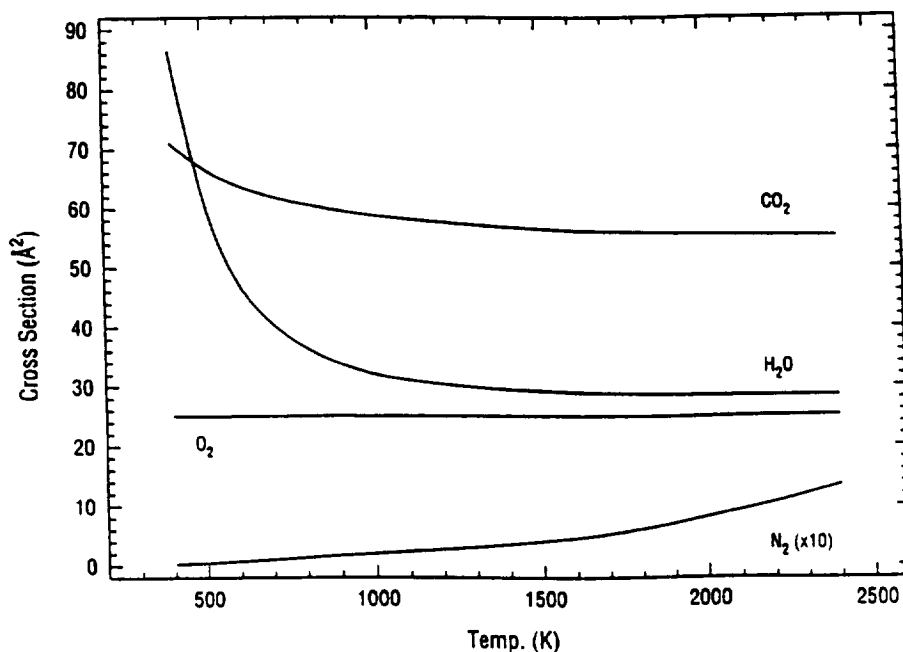
Fig. 3(b). Model calculations of collision cross-sections of various colliders with NO as a function of
temperature.
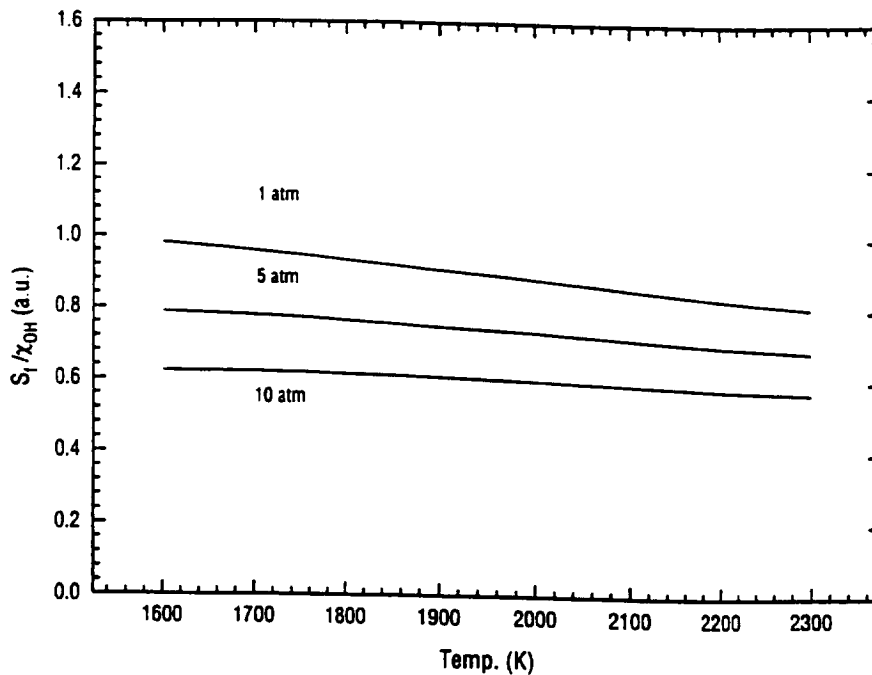
Fig. 4. OH fluorescence signal model as a function of temperature from 1 to 10 atm. Calculations are based on an equivalence ratio of 0.4, the $(1,0)P_1(8)$ transition and a laser bandwidth of $1.0 \, cm^{-1}$.

The results of these models are reproduced in Fig. 3(a) for OH and Fig. 3(b) for NO. Note that for the range of temperatures and collider species pertinent to this work (approx. 1600–2300 K) the cross-section for collisions with both NO and OH change very little with temperature.

Model Formulation Summary

Each term in Eq. (2) has now been specified in terms of known, or easily measurable global
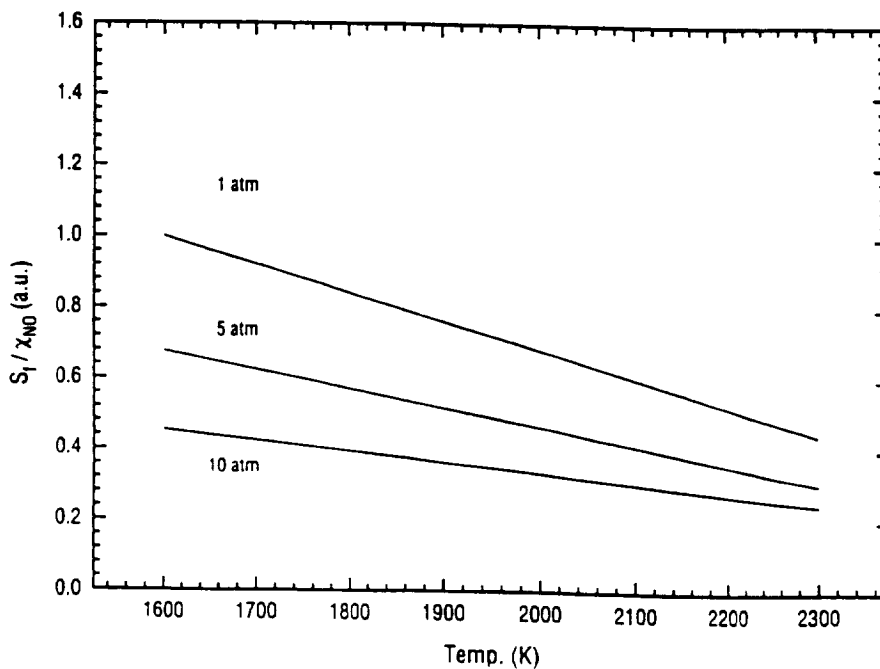
Fig. 5. NO fluorescence signal model as a function of temperature from 1 to 10 atm. Calculations are based on an equivalence ratio of 0.4, the $P_2 - Q_1(14) \, R_{12} - Q_2(21) + P_1(23)$ transition and a laser bandwidth of $0.4 \, cm^{-1}$.

parameters. The completed model of the fluorescence signal per unit absorber mole fraction can be written as:

$$\frac{S_f}{\chi_{abs}} \propto (k_{v'-j'v''j''} p) g(\phi_{abs}; \phi_{las}) \frac{1}{\frac{p}{kT} \sum_i \chi_i \sigma_i(T) \left\{\frac{kT}{\pi \mu_i}\right\}^{0.5}}. \tag{8}$$

Note that the pressure terms in the numerator and denominator cancel in this formulation (i.e., with the absorbing species expressed as mole fraction) so that the overlap integral, g, is the only remaining term which is pressure-dependent. Hence, the overlap integral must be properly accounted for in modeling the signal. Equation (8) is plotted in Figs. 4 (OH) and 5 (NO). Figure 4 shows the OH $(1, 0)P_1(8)$ transition while Fig. 5 shows the NO $(0, 0)P_{21} + Q_1(14)/R_{12} + Q_2(21) + P_1(23)$ feature.

EXPERIMENTAL DESIGN

The nature of high pressure combustion environments poses unique challenges in fluorescence experiments. These including:

- Beam attenuation due to high number density.
- Reduced signal due to increased quenching.
- Difficulty in finding an isolated transition.

These items affect the choice of transition to use, the way in which the signal is recorded and the anticipated signal-to-noise ratio.

Attenuation

High number densities can often cause considerable attenuation of the incident beam. Substantial beam attenuation results in a variation in the incident energy at each point along the beam path. This can be experimentally problematic. Therefore an absorption transition should be chosen which does not produce substantial attenuation over the path lengths (~ 2 cm) and number densities likely to be found in this work. For NO, nascent mole fractions (< 1000 ppm) are not large enough to produce 25% cm attenuation if strong $(0, 0)$ transitions are used. Therefore, weaker OH $(1, 0)$ lines are used to reduce incident beam attenuation. This band is also experimentally convenient in that the majority of the fluorescence is emitted at longer wavelengths which are well separated from a large portion of the emission. A long pass filter can then be used to reject laser scattering while still passing a substantial portion of the emitted signal.

Reduction in signal

At elevated pressures, the fluorescence signals for OH and NO are lower than at 1 atm to due to both increased quenching and the effect of the overlap integral. Since the flat burners used in this work are nearly steady, we have chosen to work with time-averaged data, collecting fluorescence signals over multiple laser shots (typically 30 shot averages).

As well, we have chosen to use simple long-pass collection filtering for the LIF model validation experiments. This type of spectral filtering, employing glass filters, helps to increase the amount of light collected and is easily integrated with planned fluorescence imaging measurements. The resulting large spectral band pass does, however, pose some problems with regard to discrimination of the fluorescence signal, as described later.

Laser bandwidth

An additional aspect of the experimental design is the choice of laser bandwidth. This parameter impacts the fluorescence signal model via the overlap integral [see Fig. 2(b)].

The variation in signal as a function of pressure is reduced as the laser bandwidth is increased. For OH, there is less than 20% difference in the model calculation from 1 to 10 atm for a bandwidth of 2.0 cm^{-1}. If a large enough laser bandwidth is used the variation in fluorescence signal per unit

mole fraction with pressure could become negligible. As well, large laser bandwidths relax the precision with which the laser must be tuned to line center. This is convenient when the molecule to be measured has an appreciable collision-induced shift of the line center frequency, as does NO. However, as the laser bandwidth increases the emitted signal decreases for the same amount of laser energy.

We have chosen to use a large bandwidth system for the OH work ($\sim 1.0\,cm^{-1}$) and a somewhat narrower system ($\sim 0.4\,cm^{-1}$) for the NO work. For NO, this produces enhanced signals at elevated pressures at the cost of having to make sure that the laser is always tuned to the transition's central frequency.

Interference

Potential interference with the spectral feature chosen can come from two sources—adjacent lines from the same species or underlying lines from other molecules. The increased line broadening at elevated pressures can cause extensive merging of adjacent spectral features. Lines at 1 atm that are well resolved may not be so at 10 atm. A well isolated line is desirable although not essential.

For the OH (1, 0), band the line spacing is sufficiently large so that several isolated features exist. Figure 6 shows a portion of the calculated OH (1, 0) spectrum near 285 nm. There appears to be no underlying interference from other molecules under the conditions encountered in this work. The well-isolated $P_1(8)$ line, at 285.685 nm, was chosen for validating the OH model.

For NO, several potential lines in the (0, 0) band exist which are sufficiently isolated for adjacent NO lines. However, the NO (0, 0) band is overlapped by high-lying lines of the O_2 Schumann–Runge system.[21] Interference form O_2 becomes important under two conditions—high O_2 concentrations and elevated pressures. Figure 7 shows portions of both the NO and O_2 spectra around 226 nm.

As indicated, the NO absorption coefficient is generally much larger that for O_2. However, in fuel-lean hydrocarbon/air flames the O_2 concentrations can often be several orders of magnitude greater than the NO concentrations. For instance, a lean CH_4/air flat flame, equivalence ratio = 0.4, can produce O_2 concentrations near 12% with NO levels less than 50 ppm.
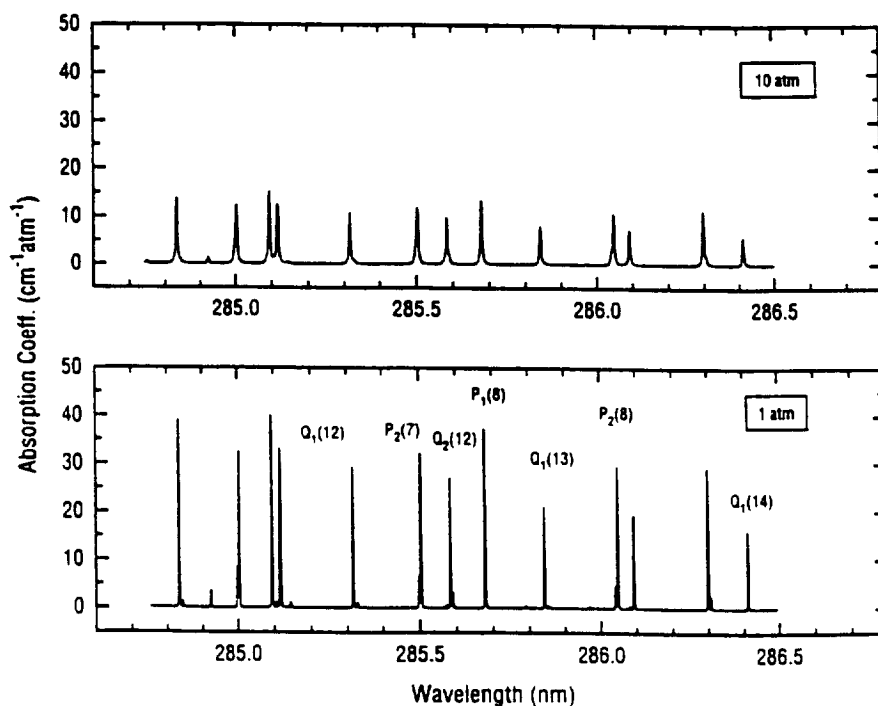
Fig. 6. Calculated OH absorption spectra for 1 and 10 atm near 265 nm. Calculations are based on experimentally observed line positions and are for 2000 K and a laser bandwidth of 1.0 cm⁻¹.
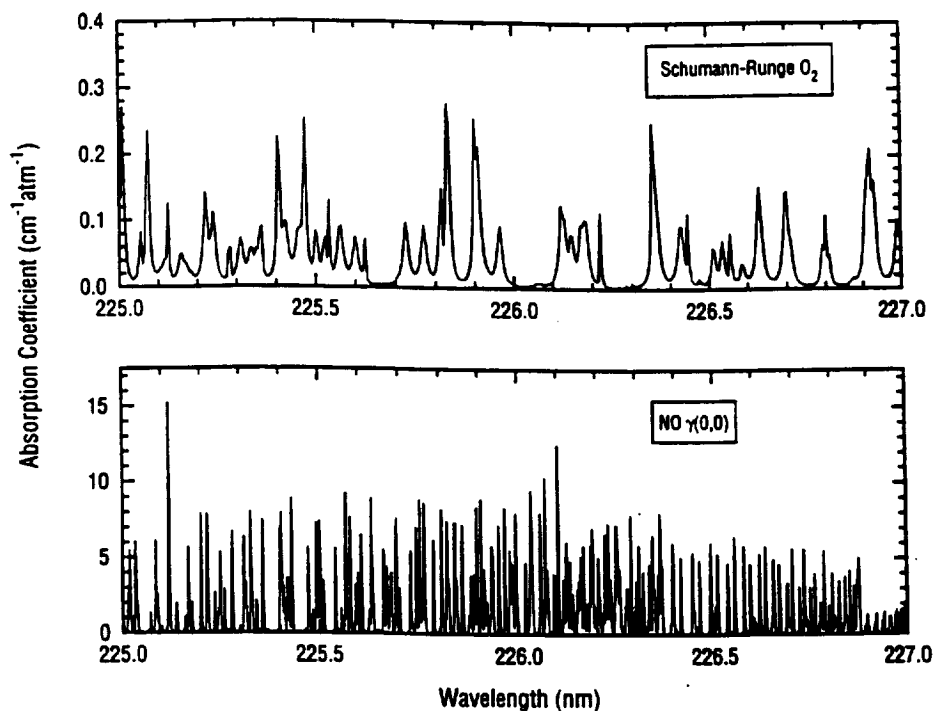
Fig. 7. Calculated NO and O_2 spectra around 226 nm. The NO line positions are based on experimental observations. The O_2 line positions are calculated from spectroscopic parameters. Calculations are for 1 atm, 2000 K and a laser bandwidth of $0.4\,\mathrm{cm}^{-1}$.

This presents two problems. First, depending on wavelength, the beam attenuation at elevated pressure resulting from O_2 can be on the order of 30%/cm. Second, the resulting fluorescence signal emitted from O_2 can be many times greater than that emitted from NO. For the O_2 transitions in this region, at the pressure pertinent to this work (1–10 atm), predissociation is the dominant
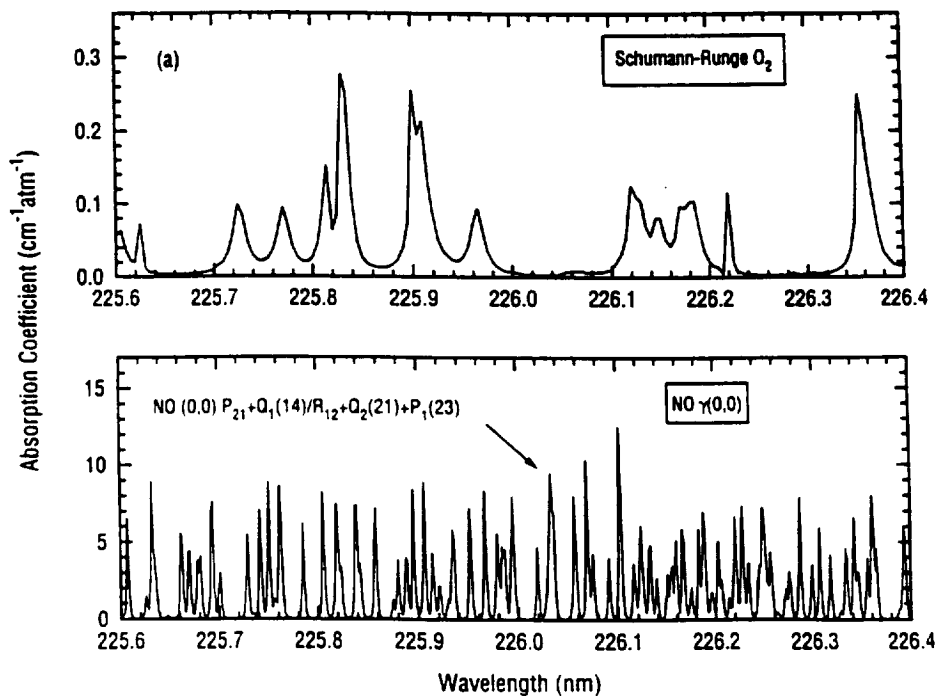
Fig. 8(a). A closer view of the calculated spectra of Fig. 7. The selected NO feature s comprised of five different transitions but is well resolved, in its entirely, at 10 atm. Note that the O_2 absorption coefficient is non-zero in the region of interest.

26

excited state loss mechanism.[26] Unlike collisional quenching, this mechanism is independent of pressure. Therefore, the O_2 fluorescence yield, and thus the emitted signal, does not decrease with pressure as does NO; in fact, the O_2 fluorescence increases nearly linearly with pressure. These factors are obstacles in making LIF measurements of low NO concentrations in lean flames at elevated pressures.

A well-defined NO feature is needed which is free from O_2 interference. As seen in Fig. 7 there are portions of the O_2 spectra where the absoption coefficient is close to but not quite zero. Several NO features coincide with these "holes". We have chosen the $(0, 0) P_{21} + Q_1(14)/R_{12} + Q_2(21) + P_1(23)$ feature, located at 226.034 nm (vacuum), to use for high pressure measurements. This feature, shown in detail in Fig. 8(a), is not a single transition but can still be treated in the model. O_2 absorption at this wavelength is only a few percent per cm even for very lean flames so that beam attenuation is not a problem in small-scale laboratory flows.

Figure 8(b) presents the results of an excitation scan near this wavelength region in a 1 atm flame with equivalence ratios of 0.4 and 1.0. In the lean flame, the large peaks are attributable to O_2 while the NO spectra around 226.000 nm are much smaller than the O_2 features. In this flame, the O_2 mole fraction was 21% and the NO level, 32 ppm. The recorded signal in the stoichiometric flame agrees well with the calculated NO spectra based on the observed line positions of Engleman et al.[23] As expected, the O_2 lines diminish in the stoichiometric flame.

Calculation and excitation scans confirm that the O_2 fluorescence signal at the wavelength of interest (226.034 nm) is minimized but not completely eliminated. The effects of the O_2 interference on the NO measurements can easily be dealt with as long as the fluorescence signal from NO is substantially greater than that from O_2. The lowest NO concentrations encountered in the 10 atm flames used in this work were approximately 50 ppm. These levels produced sufficiently large NO fluorescence signals that the O_2 signal was essentially a frequency-independent background signal. In this work, the laser was tuned off-line, to record both the NO and the O_2 background signals.

For the chosen NO feature this can be accomplished by tuning to approx. 226.015 nm where the NO spectra is near zero (see Fig. 8). Across this wavelength range (226.015–226.034 nm) the O_2 signal is nearly constant so that the O_2 contribution is effectively a background signal. This
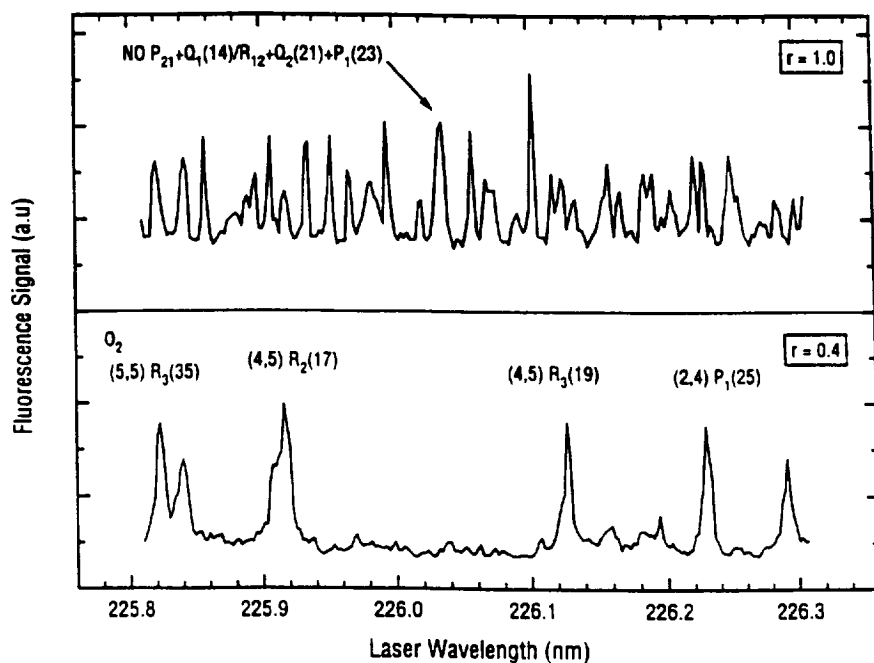
Fig. 8(b). Excitation scans in a 1 atm flame for equivalence ratios of 0.4 and 1.0. Recorded fluorescence signals are shown as the laser wavelength is scanned, using 4 mm UG5 collection filtering. Light entering the PMT was attenuated in the $r = 0.4$ case to avoid signal non-linearity. The features recorded in the top panel ($r = 1.0$) are all attributable to NO. The prominent features in the lower panel ($r = 0.4$) are identified as O_2 Schumann–Runge transitions.
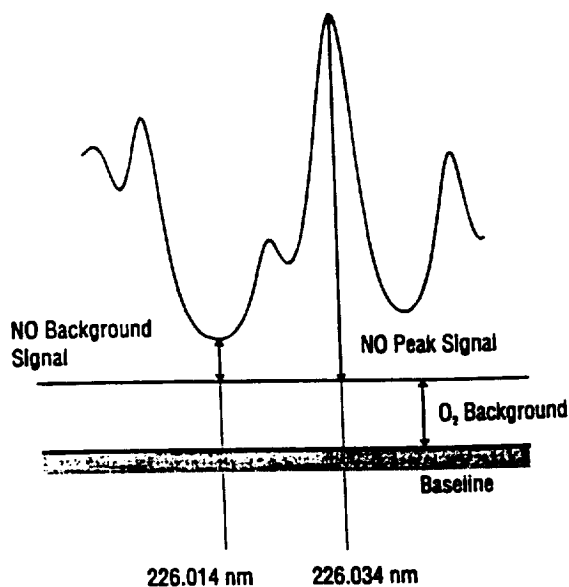
Fig. 9. Method for subtracting off the O_2 background signal by tuning away from the NO peak wavelength to 226.014 nm. This procedure results in small error for lean flames at 10 atm as long as the NO concentration is above about 10 ppm.

is shown schematically in Fig. 9. This technique is used to remove the O_2 signal contribution in the fluorescence measurements described herein.

However, the error in this method is large for lean flames, at elevated pressure, with NO levels below 10 ppm. Here, the resultant O_2 signal at the minima of the O_2 spectra at 226.034 nm is much larger than that from the low NO concentration at the peak of its spectra. This has severe implications for LIF or PLIF measurements of low NO levels in these environments. Alternatively, it is possible to record very strong LIF or PLIF images of O_2 mole fraction (and quite possibly temperature) in lean, high pressure flames, and to use the known O_2 level to correct the NO signal. The modeling of O_2 fluorescence at this wavelength and methods by which low (e.g., less than 10 ppm) NO concentrations can be measured will be discussed in a later publication.

SUMMARY

We conclude that the $OH(1, 0)P_1(8)$ line and the $NO(0, 0)P_{21} + Q_1(14)/R_{12} + Q_2(21) + P_1(23)$ feature are both suitable for single-point fluorescence at the conditions to be encountered in this work. These transitions are also suitable for PLIF imaging. Each feature is strong enough to provide adequate signal at elevated pressures while not causing consequential attenuation of the incident beam. Each feature is also sufficiently isolated such that the laser can easily be tuned to the cental frequency of the feature. For NO, the selected line minimizes interference from O_2. As well, for those situations where the O_2 background signal cannot be neglected, the laser can be tuned off the NO feature so that the background signal can be resolved.

MODEL VALIDATION EXPERIMENTS

Experimental method

The models developed for NO and OH can be validated by making experimental measurements in flames where the model parameters are known and then examining the behavior of the measured signal with that of the model. This involves:

1. Measuring temperature at a single point in the flow.
2. Measuring or calculating the absorbing species concentration at that point.
3. Acquiring single-point LIF signals at that point.

4. Measuring the laser bandwidth.
5. Using the model to infer a concentration from the LIF signal and comparing with known concentration.
6. Evaluating the comparison over a range of global parameters.

MEASURING MODEL PARAMETERS

The test facility used has been previously reported[24] and will only be summarized here. A non-premixed flat flame burner (Research Technologies, Inc. Pleasanton, CA, U.S.A.) is used to provide a spatially uniform and temporally steady source of post-flame gases. The burner is located in a pressure vessel, square in cross-section, with optical access from all four sides. Enclosed within the vessel are translation stages for positioning the burner. The flames are produced from metered flows of CH_4, O_2 and N_2 diluent. Additionally, there is an N_2 shroud flow around the burner. The burner is square with an active area of approx. 22×22 mm. The system can operate at pressures up to 10 atm with post-flame gas temperatures up to 2300 K.

Temperatures are measured using fine-gauge thermocouples which are corrected for radiation losses. Temperature are varied by changing the reactant and diluent flow rates. Pressure is measured using digital pressure transducer located below the burner.

The model validation is accomplished by making single-point measurements at the center axis of the flame, approx. 6 mm above the burner surface. At this point, the OH concentration has reached near equilibrium levels for all the conditions encountered in this work. Therefore, the OH concentration for each flame used can be determined by first measuring the temperature at this location then calculating the equilibrium composition from the known pressure and reactant mole numbers.

NO concentrations are measured with a sampling probe and chemiluminescent analyzer (CLA). The probe was fabricated from a 4 mm OD quartz tube which was drawn down to a taper and cut to produce an approx. 200 μm orifice. All NO measurements are of nascent levels in the flames used.

The sample was directed to the CLA (Thermo Electron 10-AR) through an un-heated line which included a molecular sieve water trap. The line pressure was maintained below 30 torr.

Single-point LIF measurements

For the NO work, the excitation source used was a XeCl excimer-pumped dye laser (Questek 2200 pumped Lambda Physik FL2002). Coumarin 450 dye was used and the beam frequency-doubled to ~ 226 nm in BBO, to access the NO $A \leftarrow X(0, 0)P_{21} + Q_1(14)/R_{12} + Q_2(21) + P_1(23)$ feature. For this laser, the spectral bandwidth, measured with a u.v. etalon,[25] was ~ 0.4 cm^{-1}.

For the OH work, the excitation source was an Nd:YAG-pumped dye laser (Lumonics-YM 1200 pump laser, HD 500 dye laser). This system holds several advantages over that used with NO. The Nd:YAG output power is an order of magnitude larger than that of the excimer laser, important for future PLIF imaging experiments. Also, the dye laser was customized with additional cavity optics to produce broader spectal bandwidths. This system typically was operated with an output bandwidth near 1 cm^{-1}. Rhodamine 590 dye was used and the beam was doubled in BBO to generate an u.v. output beam near 285 nm, to access the OH $A \leftarrow X(1, 0)P_1(8)$ line.

The optical scheme for single-point LIF is depicted in Fig. 10. Each beam was loosely focused over the center of the burner using a 1 m spherical lens. A portion of this beam was split and used in conjunction with a photodiode to monitor the incident pulse energy. The incident beam was attenuated ($< 100 \mu$J/pulse) to always ensure that the fluorescence was well within the linear regime, which was experimentally verified. Both lasers were operated at 10 Hz by using a master oscillator that also triggered the detection electronics.

The emitted fluorescence was focused with a 10 cm lens (1:1 imaging) onto a photomultiplier tube (PMT). For OH, a 1P28 tube (Hammamatsu) was used. For NO, and R166UH (Hammamatsu) was used. A 1 mm aperture was placed in front of the tubes to define the spatial extent of the collected signal. For OH, the recorded signal was filtered through 2 mm UG5 and WG305 Schott glass filters. For NO, a 4 mm UG5 filter was used. The PMT output signal
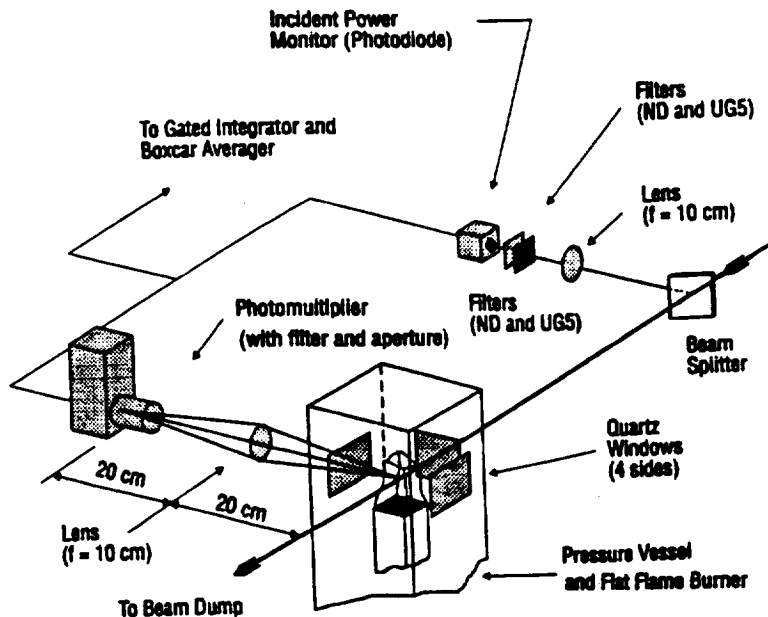
Fig. 10. Single-point LIF schematic of arrangement used to validate the fluorescence models for OH and NO.

was recorded using a gated integrator/boxcar averager (SRS 245). All single-point LIF data reported are 30 shot averages. The photodiode used to track the incident energy was also monitored in this manner. Both output signals were recorded by an i486 laboratory computer via GPIB interface.

The laser was scanned on and off line for each measurement so that a peak signal and a background signal could be recorded. For OH, the background signal was small, representing
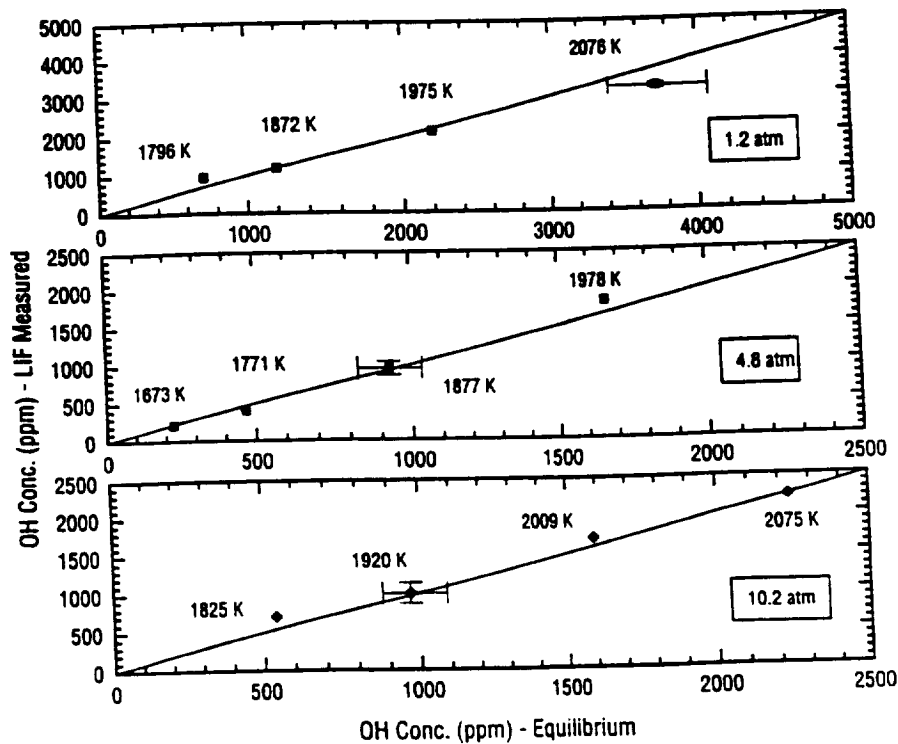
Fig. 11. Single-point model validation results for OH from LIF measurements at 285.685 nm. All data are calibrated at 1.2 atm and 1920 K.

mostly laser scattering. For NO, the background signal was somewhat larger, representing both laser scattering and residual O_2 fluorescence. Background signals were subtracted in all experiments.

Model validation results—OH

The results of the OH model validation experiments are shown in Fig. 11 for pressures ranging from 1 to 10 atm. The OH mole fraction inferred from the model-corrected and fluorescence signal is compared to the calculated OH equilibrium concentration based on the known temperature, pressure, and composition. The nominal flame equivalence ratio is 0.4. However, there is a slight variation in the product mole fractions at each point due to varying amounts of N_2 diluent flow. This is accounted for in the model calculation at each point. A single point (1 atm, 1872 K) is used as calibration for all the data.

The model-derived OH concentrations are in good agreement with the calculated equilibrium levels. This agreement, as the pressure is increased (by a factor of 10), indicates that the overlap integral has been accurately handled in the model. The agreement at any given pressure, as the temperature is changed (over a few hundred degrees K) indicates the temperature variation of both the absorption line strength and fluorescence yield have been accurately accounted for as well.

Model validation results—NO

The single-point results from the NO measurements are shown in Fig. 12. The flame conditions at each measurement point in this figure are the same as those in Fig. 11. Here, the comparison is made with the CLA-measured NO mole fractions. Again, all LIF-derived data are calibrated to the CLA at a single point. As described above, the underlying O_2 signal has been subtracted from the peak NO signal. Each data point shown represents the average of several measurements. The vertical error bars indicate the average RMS difference between the LIF data and the CLA data.

The model-inferred NO concentrations match very closely those measured independently with the CLA. The agreement with changing temperature and pressure again indicates the accuracy of the treatment of the various components of the model.
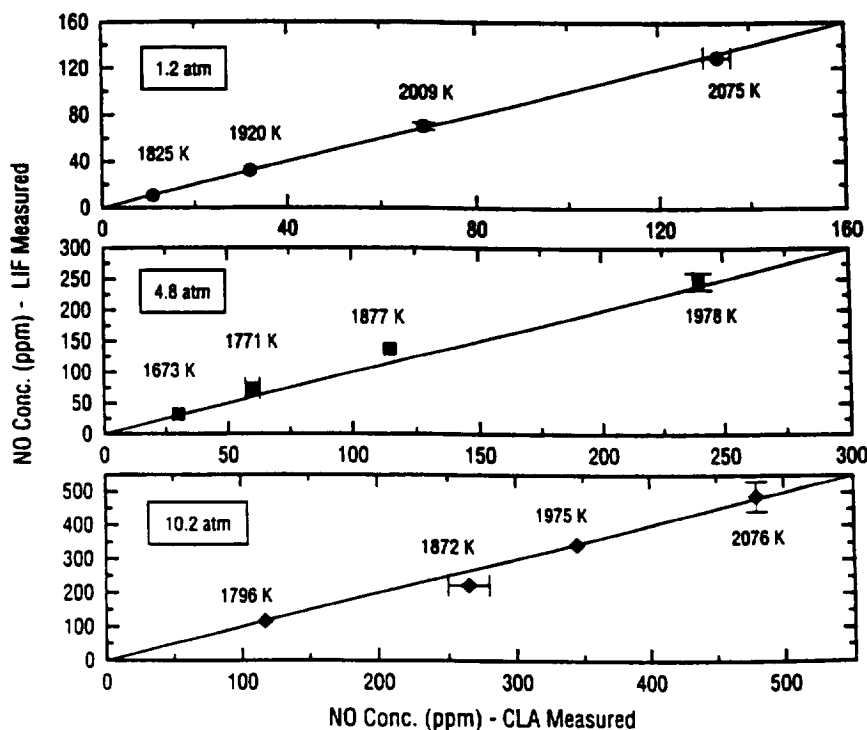
Fig. 12. Single-point model validation results for NO from LIF measurements at 226.034 nm. All data are calibrated at 1.2 atm and 1872 K.

SUMMARY AND CONCLUSIONS

In this work we have developed a quantitative model of the fluorescence signal per unit absorber mole fraction for OH and NO. The models are aimed at making quantitative corrections to fluorescence measurements in the product region of lean hydrocarbon flames at elevated pressures. The models are based on known or easily measured global parameters (temperature, pressure, overall flame equivalence ratio, and laser spectral bandwidth) and utilize the most recent published analytical studies of OH and NO collision cross-sections. Appropriate handling of the overlap integral, requiring expressions for the collision broadening, are essential in applying the model across a range of pressures.

The model agrees well with single-point measurements from 1 to 10 atm for both NO and OH. Validations were performed by making single-point fluorescence measurements approx. 6 mm above the flame front of lean ($r \sim 0.4$) $CH_4/O_2/N_2$ flames from 1 to 10 atm. Interference from O_2 Schumann–Runge transitions was minimized by judicious selection of the NO feature (226.034 nm) and by an off-line background subtraction (226.014 nm). These measurements confirmed the suitability of the models as means by which fluorescence measurements, single-point or multi-dimensional, can be used to infer species mole fraction, assuming approximate knowledge of key global parameters. This represents an important asset for the combustion scientist in that important radical concentrations can be readily inferred from fluorescence measurements.

Investigations are underway to determine methods to eliminate the O_2 contribution to the recorded signals in the NO experiments, without the need for tuning off line, and ways by which the ratio of NO to O_2 fluorescence can be improved. Included in these studies is a model of the O_2 fluorescence signal as a function of temperature, pressure, laser bandwidth and stoichiometry, at this wavelength. These efforts will aid in measuring low NO concentrations at elevated pressures in either LIF or PLIF imaging experiments. Other NO transitions, for example the (0, 1) band at longer wavelengths, show potential for reducing the O_2 interference. We are also exploring the use of high-performance special filters for separating NO and O_2 fluorescence. Such filters would possibly allow for the simultaneous recording of spectrally discriminated NO and O_2 signals in high-pressure combustion environments.

REFERENCES

1. P. H. Paul, *JQSRT* **51**, 511 (1994).
2. P. H. Paul, J. A. Gray, J. L. Durant, and J. W. Thoman, *Appl. Phys. B* **57**, 249 (1993).
3. W. R. Anderson, L. J. Decker, and A. J. Kotlar, *Comb. Flame* **48**, 179 (1982).
4. J. M. Seitzman and R. K. Hanson, AIAA Paper 92-0879, *30th Aerospace Sciences Meeting*, Reno, NV (1992).
5. R. K. Hanson, J. M. Seitzman, and P. H. Paul, *Appl. Phys. B* **50**, 441 (1990).
6. B. K. McMillin and R. K. Hanson, *Appl. Optics* **32**, 7532 (1993).
7. R. S. Barlow and A. Collignon, AIAA Paper 91-0179, *29th Aerospace Science Meeting*, Reno, NV (1991).
8. M. D. DiRosa, A. Y. Chang, and R. K. Hanson, *App. Optics* **32**, 4074 (1993).
9. E. C. Rea, A. Y. Chang, and R. K. Hanson, *JQSRT* **41**, 29 (1989).
10. B. Shirinzadeh, D. M. Bakalyar, and C. C. Wang, *J. Chem. Phys.* **82**, 2877 (1985).
11. M. Nadler and W. E. Kaskan, *JQSRT*, **10**, 25 (1970).
12. A. Y. Chang, M. D. DiRosa, and R. K. Hanson, *JQSRT* **47**, 375 (1992).
13. L. G. Dodge, J. Dusek, and M. F. Zabielski, *JQSRT* **24**, 237 (1980).
14. A. C. Eckbreth, *Laser Diagnostics for Combustion Temperature and Species*, Abacus Press, Cambridge (1988).
15. C. B. Cleveland and J. R. Wiesenfeld, *Chem. Phys. Lett.* **144**, 479 (1988).
16. R. J. Cattolica and T. G. Mataga, *Fall Meeting*, Western States Section, The Combustion Institute (1989).
17. J. B. Jeffries, D. Kohse-Höinghaus, G. P. Smith, R. A. Copeland, and D. R. Crosley, *Chem. Phys. Letters* **152**, 160 (1988).
18. M.C. Drake and J. W. Ratcliffe, Report GMR-7426, General Motors Research Laboratories, Warren, MI (1991).
19. I. S. McDermid and J. B. Laudenslager, *J. Chem. Phys.* **76**, 1824 (1982b).

20. N. L. Garland and D. R. Crosley, *21st Symp. (Int.) on Combustion*, p. 1693, The Combustion institute, Pittsburgh, (1988).
21. P. H. Kuprenie, *J. Chem. Phys. Ref. Data* 1, 423 (1972).
22. M. P. Lee and R. K. Hanson, *JQSRT* 36, 425 (1986).
23. R. Engleman, P. E. Rouse, H. M. Peek, and V. D. Baiamonte, Report No. LA-4364, Los Alamos Scientific Laboratory, Los Alamos, NM (1970).
24. B. E. Battles and R. K. Hanson, AIAA Paper No. 91-1494, 22nd Fluid Dynamics, Plasma Dynamics, and Lasers Conference, Honolulu HI, 6–9 July (1991).
25. J. L. Palmer and R. K. Hanson, AIAA Paper 93-0046, *30th Aerospace Sciences Meeting*, Reno NV, 11–14 January (1993).
26. M. P. Lee, P. H. Paul, and R. K. Hanson, *Opp. Lett.* 12, 75 (1987).

LIF Spectroscopy of NO and O₂ in High-Pressure Flames

MICHAEL D. Di ROSA, KURT G. KLAVUHN and
RONALD K. HANSON

Stanford University, High Temperature Gasdynamics Laboratory
Mechanical Engineering Department, Building 520
Stanford CA 94305-3032

We report new models of absorption, excitation, and fluorescence spectra for joint excitations of the $A \leftarrow X(0,0)$ band of NO and the $B \leftarrow X$ bands of O_2. Supporting measurements obtained from the burned regions of flames operated at pressures from 1 to 10 atm are also presented. As developed through these models, a strategy appropriate for imaging planar laser-induced flourescence is proposed that, for lean combustion environments, should afford sensitive measurements of NO concentration through the use of a single excitation wavelength despite the photolytic interference from O_2 that intensifies with increasing pressure and temperature.

INTRODUCTION

The method of laser-induced flourescence (LIF) has found extensive use in its capacity to measure non-intrusively and with good spatial resolution the concentration of nitric oxide (NO) as formed by combustion. Whether for point-wise (Westblom *et al.*, 1994; Williams and Fleming, 1994) or two-dimensional measurements [through an extension of LIF to planar laser-induced fluorescence, or PLIF (Hanson *et al.*, 1990)] of the concentration field of NO, the method traditionally employs a pulsed laser tuned to excite NO by one-photon transitions within its strong $A \leftarrow X(0,0)$ electronic system, which is centered near 225 nm. The resulting flourescence cascades in vibronic bands $A(v' = 0) \rightarrow X$ from roughly 220 to 300 nm. Though various

257

factors influence and ultimately moderate the spectral extent over which the fluorescence can be collected, it holds generally that the greater signals accompanying a broader collection bandwidth will improve the spatial resolution and detectivity of the measurement. For PLIF imaging especially, broad collection of the fluorescence distribution of NO is imperative if the method is to achieve for single-shot images a spatial resolution of $\sim 0.1\,mm^3$ (McMillin *et al.*, 1993).

With the parameters requisite for quantitative detection of NO through LIF now fairly mature (Change *et al.*, 1992; Di Rosa and Hanson, 1994a; Di Rosa and Hanson, 1994b; Paul *et al.*, 1995; Paul *et al.*, 1993), attention has turned toward assessing spectral interferences from species that have absorption and fluorescence spectra overlapping those of the $A - X$ bands (the γ-bands) of NO. In lean combustion environments, a notable spectral interference is presented by molecular oxygen, the Schumann-Runge bands $(B - X)$ of which encroach upon the $A \leftarrow X(0,0)$ absorption spectrum of NO toward high temperatures (Di Rosa and Hanson, 1994a; Wysong *et al.*, 1989) and subsequently fluoresce within the $A(v' = 0) \rightarrow X$ progression of NO. The impact of this interference is then potentially twofold, a partial attenuation of the laser beam (or sheet, in the case of PLIF) and a corruption of the NO fluorescence signal. Both effects, however, can be greatly minimized by a judicious choice of excitation wavelength while maintaining high signal levels of NO fluorescence.

Such a selection is best made by a comparison of excitation spectra, which, as a preview of the models described herein, is provided by Figure 1 for an assumed post-flame environment of 2000 K, 1 atm, 100 ppm NO, 10% O_2, plus major combustion products of CO_2, H_2O and N_2 in the respective percentages 9%, 18%, and 63%; also assumed were a tophat spectral bandpass from 230–290 nm and a Gaussian profile $0.5\,cm^{-1}$ wide (the full width at half the maximum value, or FWHM) for the spectral distribution of the laser. Between 226.0–226.1 nm there occurs a pronounced minimum in the absorption spectrum of O_2, fortuitously located where strong features of NO appear. Within this minimum and for the case represented by Figure 1, the excitation of NO at any of the five peaks labeled *a* through *e* would yield a signal ratio of NO to O_2 fluorescence of better than one hundred. Yet what appears to be a decided advantage for the broadband LIF signal of NO quickly erodes when either the pressure increases, the temperature increases, the concentration of NO relative to O_2 is substantially less, or some combination thereof. Particularly challenging, then, will be the advance of PLIF-imaging of NO to the fuel-lean, high-pressure (> 10 atm), and high-temperature ($\sim 2000\,K$) environments of gas-turbine
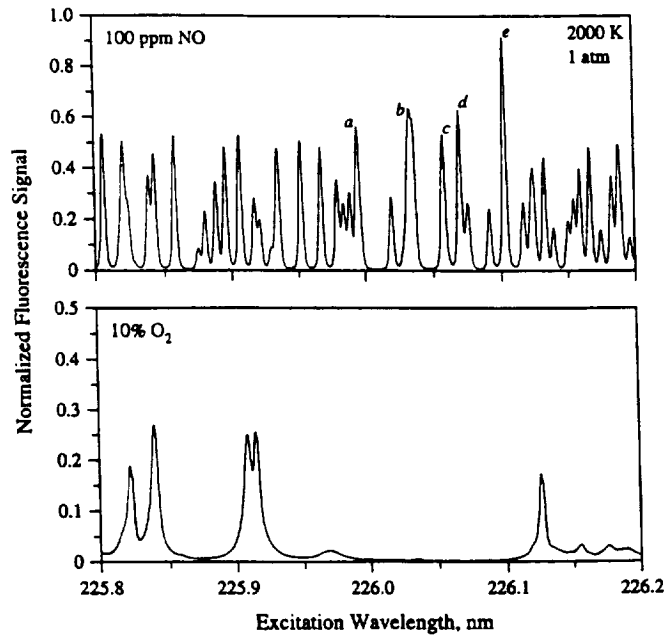
FIGURE 1 Excitation spectra of NO $A-X$ and O_2 $B-X$ as calculated for products of lean combustion (a $\phi = 0.63$ reactant mixture of $CH_4/O_2/N_2$ in the proportion 1/3.2/6.8) at 2000 K and 1 atm that include 100 ppm NO and 10% O_2. A laser FWHM of 0.5 cm^{-1} and a tophat fluorescence bandpass from 230 − 290 nm were assumed. The five labeled peaks of NO coincide with a broad, pronounced minimum in the $B \leftarrow X$ absorption spectrum of O_2.

combustors (Locke *et al.*, 1995) or their experimental analogues (Allen *et al.*, 1995), conditions for which an indiscriminate choice of excitation wavelength might severely restrict the measurement's sensitivity to NO concentration.

Because existing spectroscopic models for O_2 (Lee and Hanson, 1986) are inappropriate for very high temperatures, and because no models have apparently been assembled for the LIF spectroscopy of NO, efforts to date in the detection of NO by narrow-band LIF within the burned regions of lean, high-pressure flames have largely been empirical (Reisel *et al.*, 1994). Past work (Battles *et al.*, 1994) in PLIF conducted in our combustion facility, approached the problem of spectral interference from O_2 at high pressures by acquiring separate, sequential images of the fluorescence resulting from two different excitation wavelengths (Battles and Hanson, 1995). One image was 'on-line', obtained for an excitation wavelength at a peak of NO $A \leftarrow X(0,0)$, and the other was 'off-line' with an excitation wavelength in a nearby minimum of NO $A \leftarrow X(0,0)$. The off-line image, primarily of O_2

fluorescence, was considered a measure of the interference background that could be subtracted from the on-line image. Fairly simple to implement, this approach to PLIF imaging of NO in lean-combustion environments is nonetheless better suited to conditions of moderate pressure ($\leqslant 5$ atm) with levels of NO above 50 ppm and is intrinsically a time-averaged method unless the complexity of an additional laser system and camera is incurred.

Concern over the photolytic interference of O_2 would be eliminated by resorting to two-photon excitation of NO $A \leftarrow X(0,0)$ (unlike NO $A \leftarrow X$, $O_2 B \leftarrow X$ is two-photon forbidden), but it is preferable to exploit the joint excitation of NO and O_2 in ways that would enable not only single-shot, planar measurements of NO at ppm levels but the simultaneous measurements of the O_2 concentration and O_2 vibrational temperature as well. The method is guided by our newly-developed models for the absorption, excitation, and fluorescence spectra of NO and O_2, which are reported here together with supporting data obtained from the burned-gas regions of $CH_4/O_2/N_2$ and $CH_4/O_2/Ar$ flames operated from 1 to 10 atm.

SPECTROSCOPIC MODELS

Component formulae of the absorption and fluorescence processes are given, from which excitation spectra are synthesized. For a weak excitation by a UV laser of energy density E_0 [J/L^3] and of center frequency ω_L [rad/s], the number of absorption transitions per unit volume [L^3] from lower state i to upper state k [each state a specific $|nvJ\Omega S\Lambda\Sigma\rangle$ (Zare, 1988)] is expressed by

$$N^{abs}_{k \leftarrow i(\omega_L)} = (\Delta x/\hbar\omega_L)n_i \times \int d\omega\,\sigma_{k \leftarrow i(\omega - \omega_{k,i})}\rho_{(\omega - \omega_L)}, \qquad (1)$$

where Δx is a length [L] traversed by the beam, $\hbar$ [Js] is the Planck constant divided by 2π, n_i is the number density [L^{-3}] of the lower state (derived from the Boltzmann fraction of the state multiplied by the number density of the species), $\sigma_{k \leftarrow i(\omega - \omega_{k,i})}$ [L^2] is the cross section of absorption with center frequency $\omega_{k,i}$ and

$$\rho_{(\omega - \omega_L)} = E_0\phi_{L(\omega - \omega_L)}$$

is the laser's spectral energy density $[J/L^3/(rad/s)]$ of Gaussian distribution ϕ_L, normalized such that

$$\int \phi_{L(\omega - \omega_L)} d\omega = 1. \tag{2}$$

The cross section for an absorption transition $k \leftarrow i$ derives from

$$\sigma_{k \leftarrow i(\omega)} = (\hbar\omega_{k,i}/c) B_{k \leftarrow i} S_{k \leftarrow i} \phi_{k,i(\omega)}, \tag{3}$$

where $S_{k \leftarrow i}$ is the normalized Hönl-London factor for absorption, calculated from Earls (1935) for NO and Tatum and Watson (1971) for O_2, and $B_{k \leftarrow i}$ is the band Einstein B coefficient between the vibronic levels to which states k and i belong, related to the band Einstein A coefficient $A_{k \rightarrow i}$ $[s^{-1}]$ and the electronic degeneracies, g_j, of the connecting states through (Hilborn, 1982)

$$B_{k \leftarrow i(\omega)} = (g_k/g_i)(\pi^2 c^3/\hbar\omega_{k,i}^3) A_{k \rightarrow i}. \tag{4}$$

In Eqs. (3) and (4), c is the speed of light through vacuum. The $A_{k \rightarrow i}$ for both NO and O_2 are from Laux and Kruger (1992). An outgrowth of the Born-Oppenheimer assumption, the use of Hönl-London factors for purposes of calculating the rotational line strength is entirely appropriate for the γ-bands of NO (Scheingraber and Vidal, 1985) but only mildly so for the Schumann-Runge bands of O_2 (Gies et al., 1981). At present, however, the data and theory available on the rotational dependence of line strengths within $O_2 B \leftarrow X$ are too incomplete to justify a switch from Eq. (3).

The transition line shape, $\phi_{k,i}$, for both NO and O_2 is the Voigt profile as computed by the algorithm of Drayson (1976) with the normalization condition of unity area, as in Eq. (2). The collision widths and collision shifts of the $A \leftarrow X(0,0)$ band of NO are known from measured relations (Chang et al., 1992; Di Rosa and Hanson, 1994a; Di Rosa and Hanson, 1994b) for perturbers Ar, N_2, O_2, and H_2O – four of the six major constituents of the product gases considered here. The other two species, CO and CO_2, lack comparable studies but can be, to a very good approximation, assumed identical to N_2 in the broadening and shift they collisionally induce in the $A \leftarrow X(0,0)$ transitions of NO. For transitions of the Schumann-Runge bands of O_2, the homogeneous width for the conditions investigated is primarily from predissociation, and account is taken here of the vibrational, rotational. and fine-structure dependence of the predissociation linewidths

(Lewis *et al.*, 1994). Collisional broadening (Δv_c) and shift (Δv_s) of transitions within the Schumann-Runge bands become evident toward high pressures (*P*) and are currently estimated from the relations

$$\Delta v_c|_{\text{FWHM O}_2} \ [\text{cm}^{-1}] = (0.21) \times (P[\text{atm}]) \times (273.2/T[\text{K}])^{0.7}$$

$$\Delta v_s|_{\text{O}_2} \ [\text{cm}^{-1}] = (-0.063) \times (P[\text{atm}]) \times (273.2/T[\text{K}])^{0.7}$$

which comprise the room-temperature coefficients of Lewis *et al.* (1988) and their extrapolation in temperature (*T*) as drawn from simple theory (Breene, 1961; Di Rosa and Hanson, 1994b). The line shape of a transition in the direction of fluorescence is assumed equal to the line shape in abosrption. Line-shape parameters for the $A(v'=0) \to X(v''>0)$ fluorescence transitions of NO are set equal to those of the A–$X(0,0)$ band.

   With reference to Eq. (1), the number of LIF photons per unit volume and per unit frequency occuring by spontaneous emission from upper state *k* to a lower state *j* may be experessed (in the limit of zero energy transfer within the upper state) by

$$N^{fl}_{k \to j (\omega, \omega_L)} = \varepsilon^{fl}_{k \to j} N^{abs}_{k \leftarrow i (\omega_L)} \phi_{k,j(\omega)} \,, \tag{5}$$

where the dimensionless quantity

$$\varepsilon^{fl}_{k \to j} = A_{k \to j} S_{k \to j} \bigg/ \left(Q_{\text{elec}} + Q_{\text{pred}} + \sum_i A_{k \to i} \right) \tag{6}$$

is the fluorescence quantum efficiency. A relation alternate to Eq. (5), and perhaps a more useful one from a practical standpoint, is formed by setting the dimension [*L*] to centimeters, the length Δx to 1 cm, the laser energy density (E_0) to $1 \, \text{mJ/cm}^3$, integrating Eq. (5) over a volume $1 \, \text{cm}^3$ (1 cm pathlength $\times$ 1 cm^2 cross section) through which passes 1 mJ of laser energy, and including a divisor or 4π (the surface area of the unit sphere). The net result is termed here the 'spectral LIF yield', which gives the number of LIF photons per mJ of laser energy per cm of path length per unit bandpass (either frequency or wavelength, depending on how one integrates over $\phi_{k,j}$) and per unit solid angle.

   As written, Eqs. (5) and (6) omit influences of non-radiative processes other than electronic quenching and predissociation, the rates for which are represented by Q_{elec} and Q_{pred}, respectively. The summation over $A_{k \to i}$ is, for

39

both NO and O_2 at the conditions of interest here, a very minor term in the denominator of Eq. (6) and appears for completeness only. For the $A(v' = 0)$ level of NO, $Q_{pred} = 0$, Q_{elec} is calculable for flame environments (Paul *et al.*, 1995; Paul *et al.*, 1993), and vibrational relaxation is safely ignored. Rotational relaxation within the $A(v' = 0)$ level of NO is discernible in the environments studied but incomplete enough to justify its omission for present purposes. The electronic quenching rate for the *B*-state of O_2 is unknown, but it is suspected that the predissociation of O_2-*B*, with a rate of roughly $5(10^{10})s^{-1}$, predominates quenching for pressures up to 10 atm [for comparison, Q_{elec} for NO $A(v' = 0)$ in the burned region of a CH_4/air flame at 10 atm is only one tenth the nominal predissociation rate of the *B*-state of O_2]. Still, as a crude account, the quenching rate of any ro-vibrational level of O_2-*B* is assumed equal to that affecting rotational states within the $A(v' = 0)$ level of NO. Rates of rotational and vibrational relaxation of the *B*-state O_2 are also unknown, and their absence from the model is justified solely empirically from measurements of dispersed fluorescence for pressures up to 10 atm at temperatures of nominally 2000 K. Apparently, for the conditions and excitations particular to these measurements, processes of rotational-energy and vibrational-energy transfer are still masked by predissociation.

Transition energies for the $B^3\Sigma_u^- - X^3\Sigma_g^-$ bands of O_2 were calculated by the formulae of Miller and Townes (1953) with spectroscopic constants drawn from Nicolet *et al.* (1989), Creek and Nicholls (1975), and Fang *et al.* (1974). These sources, along with minor interpolations and extrapolations, permitted calculations of line positions connecting $0 \leqslant v'' \leqslant 19$, $0 \leqslant N'' \leqslant 45$ with $0 \leqslant v' \leqslant 14$, $0 \leqslant N' \leqslant 46$. Line positions of the $A(v' = 0) - X(0 \leqslant v'' \leqslant 7)$ bands of NO were determined for $0 \leqslant J'' \leqslant 65$ by methods outlined elsewhere (Chang *et al.*, 1992), along with supplemental spectroscopic constants from Engleman *et al.* (1970) and Engleman and Rouse (1971) [see Di Rosa (1996) for details].

EXPERIMENTAL VALIDATION

The experiment, diagrammed in Figure 2, includes a windowed high-pressure combustion facility and Nd:YAG-pumped laser system (a Lumonics Model YM-1200 Nd:YAG laser, a Lumonics Model HD-500 dye laser running Coumarin 430 dye and pumped by the 3rd harmonic of the ND:YAG laser, and a Lumonics Hyper Trak 1000 for single-pass frequency-doubling of the dye-laser fundamental) that delivers 10 ns pulses at
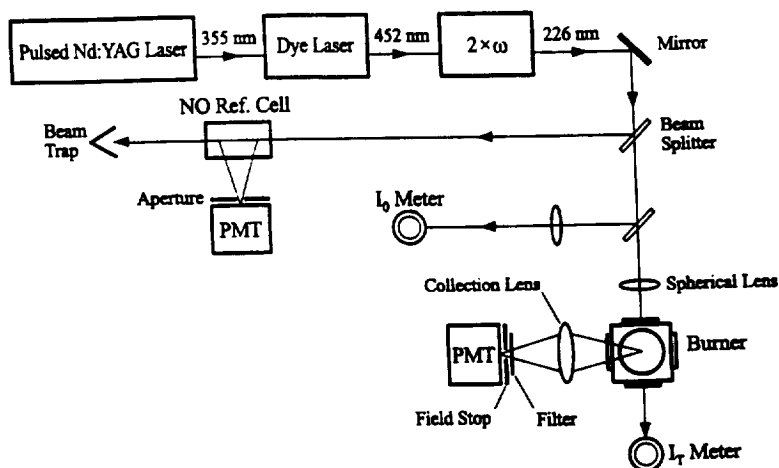
FIGURE 2   Experimental schematic for measurements of excitation spectra. Measurements of the fluorescence spectra were approached similarly but with a monochromator in place of the filtered PMT.

10 Hz of laser light tunable from 220–230 nm. Operable from 1 to 12 atm, the combustion facility consists of a non-premixed burner centered within a stainless steel pressure vessel of square cross section 11 × 11 cm. On each side of the chamber and centered about the rim of the burner is a mount of clear aperture 4.5-cm square to which either a window (9.5-mm-thick UV-grade fused silica plates) or a thermocouple probe (as sealed to an aluminum blank) can be secured. The burner (from Research Technologies, Inc.), a 2.5 × 2.5 cm honeycomb grid of separate channels for fuel and oxidizer arranged hexagonally with each fuel channel touching six oxidizer channels, flows CH_4 and O_2 with either N_2 or Ar as a diluent. All gases are of research grade (purity $\geqslant 99\%$) and are metered individually by mass flow controllers. The roughly 200 diffusion flamelets generated by the burner merge to form a dimpled but contiguous flame sheet close to the burner surface, above which the gases mix and homogenize to yield laterally-uniform product distributions at temperatures of up to 2000 K. A uniform shroud of N_2 purges the peripheral area of combustion products, mainly to displace the cold NO and ensure the outer regions are transparent at the laser wavelength but also to shield the windows from deposits of soot. The laser beam, of $\sim$ 1 mm waist, traverses the chamber at a height of roughly 1 cm above the burner surface, its energy reduced as necessary to operate well within the weak excitation limit (*i.e.* within the 'linear-fluorescence'

regime. where the laser energy and fluorescence signal are directly proportional). At the burner, laser energies are typically $30\,\mu J$/pulse.

The laser-induced fluorescence is collected at $90°$ from a small segment of the beam directly above the burner's center. At this location the temperature is measured with a Pt/Pt-13% Rh (type R) thermocouple of bead diameter $\sim 250\,\mu m$. Inclusive of a correction for radiation losses (Bradley and Matthews, 1968), the thermocouple voltage is converted to a measurement of the gas temperature with an estimated uncertainty of $\pm 40\,K$. For producing excitation scans, the laser frequency is scanned, and the fluorescence is imaged onto a photomultiplier tube (PMT) after passing through a spectral filter. The fluorescence spectrum for a fixed laser frequency is obtained through use of a $0.5\,m$ monochromator, equipped with a 2400 groove/mm grating and a PMT at the exit plane, that is calibrated for wavelength accuracy and spectral sensitivity.

Serving as a reference for the laser frequency is the record of an excitation scan of NO at room temperature—simultaneous with excitation scans of the flame environment, anterior to measurements of the fluorescence spectra—produced by directing a small portion of the incident beam through a cell filled to ~ 300 torr with a mixture NO/N_2 and detecting the fluorescence with a PMT. A comparison of the reference excitation spectra with a synthetic one based on known line positions (Engleman et al., 1970) determines the laser frequency to an accuracy of better than $|0.1\,cm^{-1}|$. Incident (I_o) and transmitted (I_T) energies of the laser beam are monitored in order to account for the minor attenuation of the beam on its way to the measurement volume. All signals are recorded by gated integrators (Stanford Research Systems Model SR250) and then transferred to a computer for analysis.

Excitation Spectra

Examples of measured excitation spectra of the $B{\leftarrow}X$ bands of O_2 are shown in Figures 3 and 4 for conditions of $1920\,K/1.2\,atm$ and $2020\,K/10.4\,atm$, respectively. Both conditions were generated by lean CH_4/O_2 flames with Ar as the diluent (as opposed to N_2) in order to examine the O_2 spectra without complications from NO; flowrates of the reactants were nominally 0.9 slpm for CH_4, 5.9 slpm for O_2, and 6.6 slpm for Ar. In both figures, the abscissa is the vacuum laser-wavelength, and the ordinate is the (normalized) fluorescence signal as filtered in wavelength by a bandpass extending in FWHM from approximately 240–270 nm, defined by the spec-
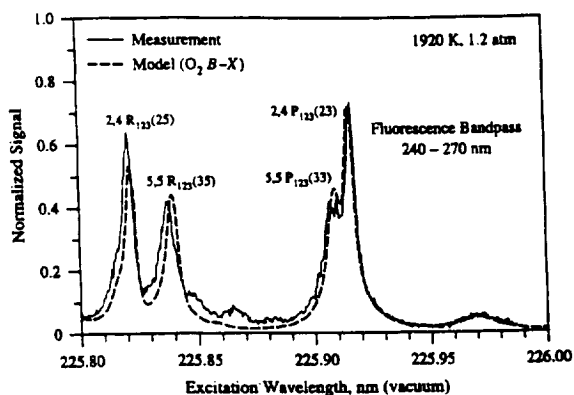
FIGURE 3   Measured and modeled excitation spectra of $O_2 \, B-X$ for flame conditions of 1920 K and 1.2 atm, a spectral bandpass from 240–270 nm, and a laser FWHM of 0.5 cm^{-1}.
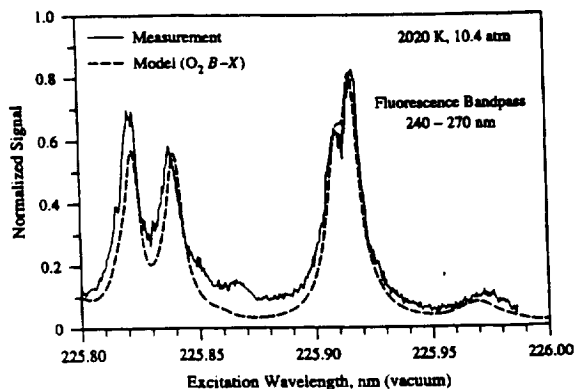
FIGURE 4   Measured and modeled excitation spectra of $O_2 \, B-X$ for flame conditions of 2020 K and 10.4 atm, a spectral bandpass from 240–270 nm, and a laser FWHM of 0.5 cm^{-1}.

tral response of the PMT and the transmission function of the interference filter preceding it. Each excitation spectrum was modeled by evaluating, for a given discrete step of the laser wavelength and for each transition promoted by the laser, whose spectral distribution was reasonably estimated as a Gaussian of 0.5 cm^{-1} FWHM, the integral over ω of Eq. (5) weighted by the known spectral bandpass. The vertical scale of the synthesized spectrum was then multiplied by a constant as required to match the measurement at a prominent feature. In Figure 3, for instance, the model was normalized relative to the measured peak at ~225.915 nm, composed mainly of the

triplet $2.4\,P_1(23)$ plus $2.4\,P_2(23)$ plus $2.4\,P_3(23)$, abbreviated in Figure 3 by $2.4\,P_{123}(23)$. [Transitions are described by the conventional shorthand v', $v''\,\Delta J(N'')$, with P, Q, and R for $\Delta J = J' - J'' = -1, 0$, and 1, respectively.] Main contributors of three other peaks are also labeled.

The overall exceptional agreement seen in Figure 3 between the measured and modeled spectra lends confidence in the spectroscopic parameters incorporated for calculations of the absorption and fluorescence spectra of the $B-X$ bands of O_2. Especially important is an account of the spin-dependence of the predissocation widths (Lewis *et al.*, 1994), without which the modeled excitation spectra would err significantly, possessing structure and peak ratios irreconcilable with the measurements. Toward high pressures, where collisional broadening becomes evident by the increased blending of features, the model maintains its good overall agreement with the measurement as seen in the (~ 10 atm) case of Figure 4. The disparity between the model and measurement near and about 225.87 nm, seen more pronounced in the higher-temperature case of Figure 4, is likely from the emergence of high-lying rotational states that are beyond the limits and safe extrapolation of the current data base.

Excitation spectra of sections of the $A \leftarrow X(0,0)$ band of NO were obtained similarly, though fuel-rich stoichiometries of $CH_4/O_2/N_2$ were instead used to minimize the concentration of O_2 in the post-flame gases. For cases at 1 to 10 atm, the measured spectra were capably predicted by the model, thus confirming the collision widths and collision shifts of the $A \leftarrow X(0,0)$ transitions of NO measured previously (Chang *et al.*, 1992; Di Rosa and Hanson, 1994a; Di Rosa and Hanson, 1994b). An example of their comparison is shown in Figure 5 for conditions of 1840 K and 10.6 atm, with some of the peaks labeled and by nomenclature similar to that parenthetically described for transitions of O_2.

Fluorescence Spectra

A complement to broadband excitation spectra, which are compounds of the absorption spectra and the fluorescence quantum yield, fluorescence spectra serve to test more precisely the modeled fluorescence distribution and also to reveal possible routes of energy redistribution in the upper state. At flame conditions similar to those used for measurements of the excitation spectra, the fluorescence spectra of O_2 and NO were examined separately by fixing the laser wavelength, typically on a prominent absorption feature, and scanning the monochromator. The relative spectral response (RSR) in
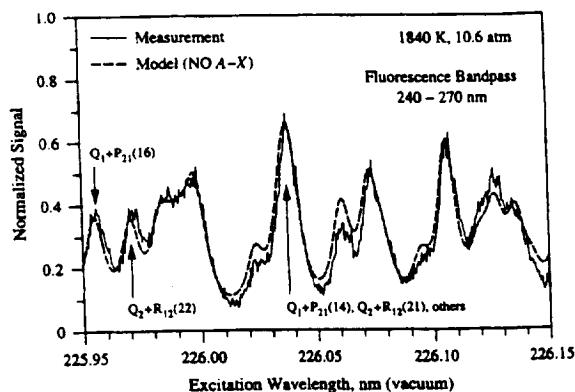
FIGURE 5   Measured and modeled excitation spectra of NO $A-X$ for flame conditions of 1840 K and 10.6 atm, a spectral bandpass from 240–270 nm, and a laser FWHM of 0.5 cm^{-1}.

the UV of the monochromator, collection lens, and chamber window combined was established through the use of a calibrated D_2 lamp. Converted to a basis of signal/photon, the RSR of the complete system peaked at 325 nm, falling smoothly to 1/3 and 2/3 of this peak value at 230 nm and 360 nm, respectively. For measurements of the fluorescence spectra, the slit widths of the 0.5 m monochromator were each set to 200 µm, which with its 2400 groove/mm grating lent a measured FWHM instrument width of 1.84 Å.

Because the Schumann-Runge bands near 226 nm are an overlapping assemblage of vibronic bands with lines of large (~ 3 cm^{-1}) predissociation widths, a laser beam with a wavelength in this vicinity quite generally excites dozens of O_2 transitions. There are, however, many instances where the laser excites primarily just two or three rotational lines and therefore engenders a fluorescence spectrum that is easier to interpret. One instance is depicted in Figure 6, which shows a segment of the calculated absorption spectrum of O_2 $B-X$ and the two constituent 'lines', the blended features of $7,6\,R_{123}(25)$ and $2,4\,R_{123}(25)$, that compose the peak at 226.821 nm. In the absence of energy transfer within the upper state, an excitation at 226.821 nm would then give rise to a fluorescence spectrum stemming mainly from upper-state levels ($v' = 7$, $N' = 26$) and ($v' = 2$, $N' = 26$). The measured fluorescence spectrum of O_2 induced by this excitation wavelength, and for conditions of 2020 K, 10.6 atm, is shown in Figure 7a, this to be compared with Figure 7b, a synthetic fluorescence spectrum based on the same experimental conditions, convolved with the known instrument width, and normalized at 260 nm to the measured spectrum. Though the highly
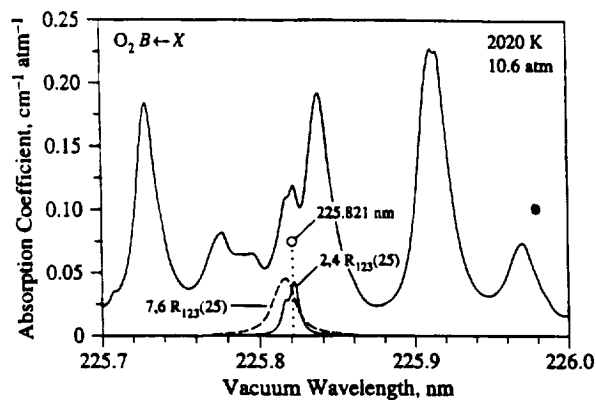
FIGURE 6 Calculated absorption spectrum of $O_2 B-X$ at 2020 K and 10.6 atm showing the constituent lines excited by a laser at 225.821 nm.
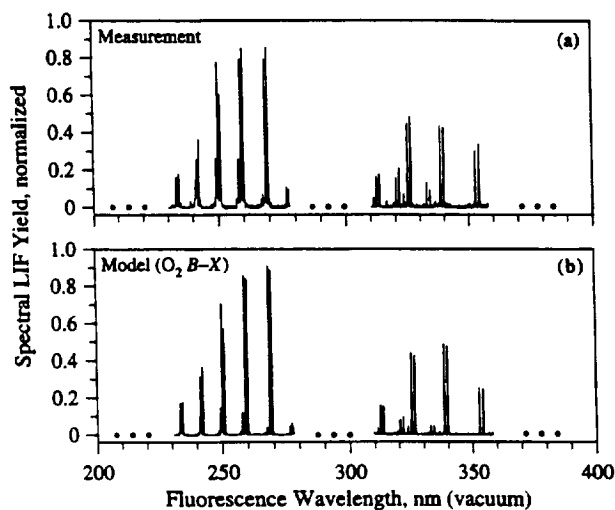
FIGURE 7 Fluorescence spectrum of O_2 $B-X$ for conditions 2020 K and 10.6 atm as induced by laser excitation at 225.821 nm and of 0.5 cm^{-1} FWHM. (a) measurement. (b) model.

non-diagonal Franck-Condon matrix of the $B-X$ system of O_2 makes for an LIF spectrum that extends from the vacuum UV through the visible, measurements were limited to those sections of interest in the '2-zone' approach to PLIF discussed in the next section.

In terms of line position and overall envelope, the model satisfactorily predicts the measured fluorescence spectrum of Figure 7. Also, the absence in the measured distribution of structure extraneous to the model indicates that predissociation, at least for the upper states involved here, still outstrips processes of energy transfer in the B-state of O_2 in combustion environments at 10 atm. A closer inspection of the two spectra, provided by Figure 8, reveals however a disparity between the measured and modeled magnitudes of fluorescence. Relative to the fluorescence emanating from upper state ($v' = 2$, $N' = 26$), the fluorescence stemming from ($v' = 7$, $N' = 26$) is, for each band observed, underpredicted by (roughly) a factor of two. Possible contributors to this disparity include the inaccuracy for the O_2 $B-X$ system of Hönl-London factors for determining the rotational line strength and a slight ($< 1 \, cm^{-1}$) difference between the true and calculated frequency separation of absorption transitions $7,6 R_{123}(25)$ and $2,4 R_{123}(25)$.

In a similar fashion, the dispersed LIF of the $A(v' = 0) \rightarrow X$ system of NO was measured at conditions 1900 K and 10.6 atm for an excitation wavelength of 226.036 nm, a wavelength near the central peak labeled in Figure 5. A portion of the measured spectrum is shown in Figure 9 along with modeled results of the LIF distribution for the two limiting cases of rotational energy transfer (RET), the solid line for zero RET within $A(v' = 0)$ and the dashed line for full rotational equilibration (termed full RET), an assumption appropriate only when the rate of RET is very much larger than rates of other processes of relaxation or de-excitation. Compared with the full- and zero-RET models, the measured LIF spectra shows the struc-
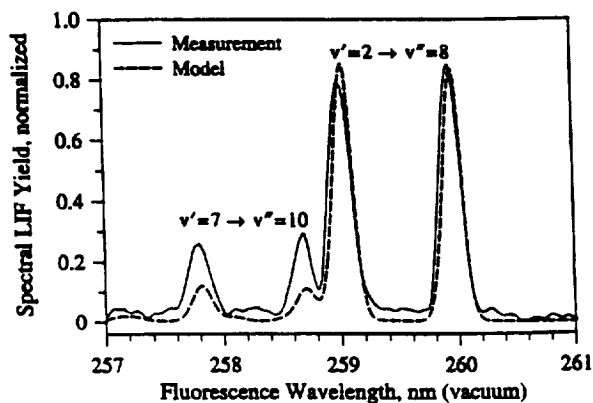
FIGURE 8   Portion of Figure 7 providing a closer inspection of the measured and modeled LIF spectra.
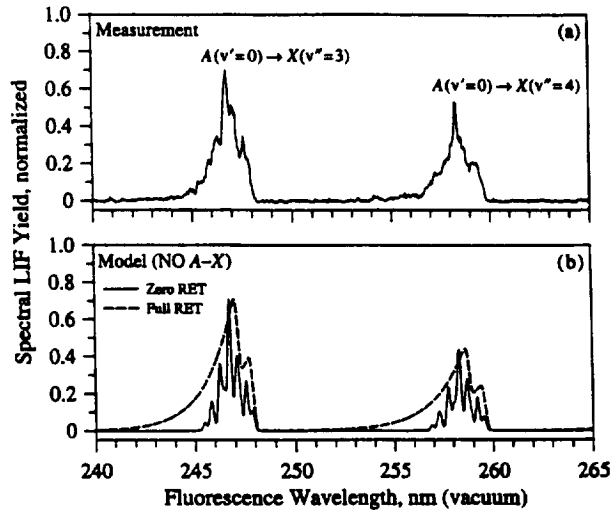
FIGURE 9   Fluorescence spectrum of NO $A-X$ for conditions $1900\,K$ and $10.6\,atm$ as induced by laser excitation at $226.073\,nm$ and of $0.5\,cm^{-1}$ FWHM. (a) measurement. (b) synthetic spectra for assumptions of zero RET and full rotational equilibration (full RET) in NO-A.

ture of a partial equilibration and a shape closer to the case of zero-RET. This closer accord with the zero-RET assumption is not surprising. While for the $A(v' = 0)$ level of NO the state-to-adjacent-state rate of RET in these flames is roughly ten times (Mallard *et al.*, 1982) the rate of electronic quenching (Paul *et al.*, 1995; Paul *et al.*, 1993), this advantage is hardly sufficient for thermalizing through the sequential process of RET a singular deposit of energy in the time allotted by quenching. Though observed for the specific case of 10.6 atm, the better applicability of the zero-RET for NO model holds for flame environments in general because the ratio of the rate of RET to quenching is independent of pressure.

MULTI-ZONE DETECTION

For excitations of the $A \leftarrow X(0,0)$ band of NO in the presence of O_2 at high temperatures, a broad bandpass filter positioned spectrally to capture the fluorescence of NO will invariably collect fluorescence from O_2, which extends quite broadly over the fixed cascade of NO $A(v' = 0) \rightarrow X(v'')$ as well as to wavelengths much shorter and longer. Possibly, then, the signal from O_2 in a second spectral region exclusive of NO would provide an indirect

measure of oxygen's portion of the total signal captured by a bandpass intended for NO. Under certain conditions, a measure of the vibrational temperature of O_2 might too be derived, this by a ratio of fluorescence signals obtained from regions flanking the LIF distribution of NO.

With regard to the detection of trace amounts of NO in high-pressure flames by (P)LIF-based methods that rely on broadband collection for high signal levels, fixed nonetheless is the primary goal of minimizing as much as possible the interference posed by O_2. This requirement we maintain while in addition offering a method for achieving, if necessary, ppm sensitivity of NO at flame conditions of 10 atm through spectral division of the fluorescence generated with each laser pulse.

A measurement of the broadband LIF signal of NO, one with a simultaneous account of the interference signal from O_2, requires the minimum acquisition of two separate spectral channels or regions, the assignment of which is straightforward from a practical standpoint. One region must encompass the bulk of the LIF from NO (while rejecting laser scatter at ~ 226 nm), and the other should enclose fluorescence from O_2 exclusively. This second region we choose at wavelengths longer rather than shorter than the first to remain where losses through transmissive optics are low and absorption by the gas negligible. As denoted by the shaded areas of Figure 10, which shows the modeled LIF spectra of NO and O_2 for a particular excitation wavelength near 226 nm, we demarcate the two regions by ideal 'tophat' bandpasses, with region 1 covering 230–290 nm and region 2 from 310–400 nm. Put simply, the fluorescence signal from region 2 relates the amount of signal from O_2 contained by region 1, an approach termed here the '2-zone' method.

The remaining consideration is that of excitation wavelength, chosen to excite NO at a peak within its $A \leftarrow X(0,0)$ band but also with criteria of minimizing *i*) the signal ratio of O_2 to NO within region 1, *ii*) the temperature dependence (from 1800 – 2200 K) of the ratio of O_2 signals in regions 1 and 2, and *iii*) the temperature dependence (from 1800–2200 K) of the NO signal. Our calculations indicate that, for combustion environments at 10 atm, a good compromise among these criteria is offered for an excitation wavelength of 226.073 nm (an excitation of peak *d* of Fig. 1), the LIF spectra induced by which (for a laser of spectral width 0.5 cm^{-1} FWHM) is shown on an absolute scale in Figure 10 for conditions 2000 K, 10 atm, 10% O_2, 10 ppm NO, and a balance of the major products CO_2, H_2O, and N_2 in the respective percentages 9%, 18%, and 63%.

The variation with temperature of what would be proportional to the broadband LIF signals of NO and O_2 appears in Figure 11, which, for

49
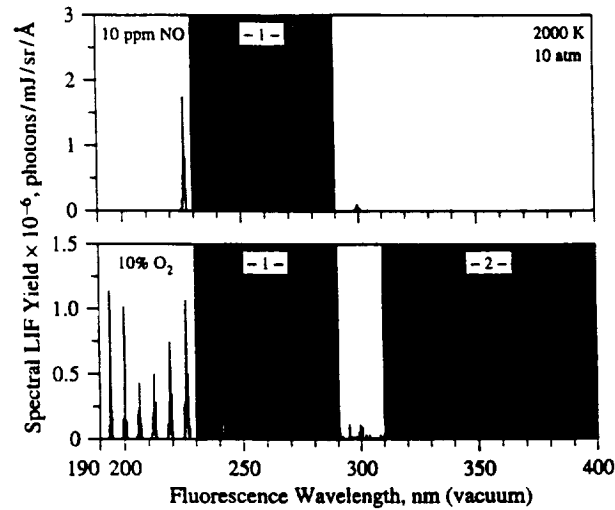
FIGURE 10   Calculated fluorescence spectra of NO $A-X$ (top panel) and O_2 $B-X$ (bottom panel) for an excitation wavelength of 226.073 nm, a laser of spectral width 0.5 cm^{-1} FWHM, an ambient gas of major combustion products at 2000 K and 10 atm including 10 ppm NO 10% O_2, and a FWHM collection bandwidth of 1 Å. Widths of shaded areas demarcate zones of fluorescence collection.
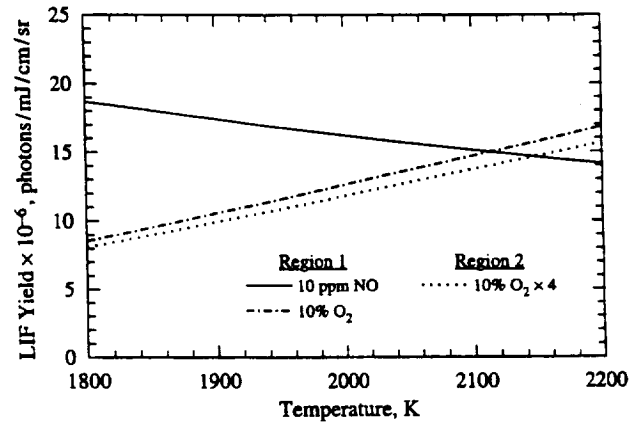
FIGURE 11   Temperature variation of the LIF yields of NO and O_2 as spectrally-integrated across regions 1 and 2 shown in Figure 10. Other than the variable temperature, the gas conditions stated in the caption of Figure 10 apply.

conditions otherwise identical to those assumed for Figure 10, gives the component LIF yields of NO and O_2 as spectrally-integrated over regions 1 and 2. As seen, the LIF yield of NO in region 1 exceeds that from O_2 over

50

most of the temperature range 1800–2200 K. Also, the LIF yields from O_2 in regions 1 and 2 maintain a nearly constant ratio of 4:1. By extension, the component LIF signals from O_2 would also remain fixed in proportion. The interference lent by O_2 to the total signal of region 1 is then subtracted as simply a constant of the signal measured for region 2, and the LIF signal from 10 ppm of NO in region 1, obscured in this case by signal of nearly equal strength, becomes fairly unshrouded.

Systematic errors are thus greatly reduced. For illustration, we assume the overall conditions are those associated with Figure 11, that the temperature ranges randomly (as a uniform variate) and unknowingly between 1800–2200 K, and that the detection system has been calibrated at 2000 K for what are presumed to be constants of *i*) the conversion of NO signal to NO mole fraction (in region 1) and *ii*) the signal ratio of O_2 as split between the two regions. If not removed, the signal from O_2 in region would present, converted to a basis of NO mole fraction, a minimum systematic bias of 8 ppm. The gradual decline in the signal of NO with increasing temperature would be unwittingly compensated by the attendant increase in signal from O_2, mitigating the random 'noise' to a perceived ± 1 ppm (an intrinsic lower bound and not one inclusive of experimental sources, such as shot noise). However, because the ratio linking the signals of O_2 in regions 1 and 2 varies with temperature less than $\pm 1\%$ from its value at 2000 K, the interference may be subtracted with very good certainty based on the signal of region 2. Detectivity would then improve to levels of a few ppm of NO from its former limit of one to two times the unaccounted systematic bias of 8 ppm. What remains for error (again apart from experimental sources) is the uncertainty incurred by assuming the signal from NO is independent of temperature. As referenced to 2000 K, we find from Figure 11 that the LIF signal from NO varies $\pm 15\%$ from 1800 to 2200 K. Levels of 10 ppm of NO could thus be measured in 10-atm fuel-lean combustion environments with, in principle, as little error as ± 2 ppm, this while maintaining the high-signal levels afforded by broadband collection, the simultaneity requisite of 'single-shot' methods, and an economy of laser use.

Applied to PLIF-imaging, the 2-zone method could proceed with two cameras, each appropriately filtered, that would oppose one another and image the fluorescence sheet from either side. If optical access for imaging is limited to a single port, the arrangement presented in Figure 12 might be used instead. A dichroic filter, one that (when aligned at a 45° angle-of-incidence) reflects $\lambda > 300$ nm but transmits $\lambda < 300$ nm, is inserted first, followed by the cameras with their associated filters positioned accordingly along the reflected and transmitted legs.

51
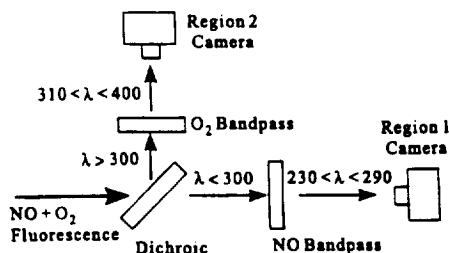
FIGURE 12   Proposed implementation of the 2-zone method.

As described, the 2-zone method is applicable to environments of variable oxygen mole fraction because of the constant proportionality, independent of temperature, maintained by the oxygen signals in regions 1 and 2. Taken individually, however, the magnitude of each oxygen signal is strongly dependent on temperature, increasing twofold for the 20% increase in temperature from 1800–2200 K (see Fig. 11). Therefore, the O_2 signal of region 2 may be converted to temperature for cases where the mole fraction of O_2 is reasonably uniform across the imaged area. The temperature so inferred (for the specified excitation wavelength) is strongly tied to the ground-state population of $v'' = 5$; the fluorescence in region 2 (and in region 1) stems primarily from vibrational level $v' = 4$ as populated by absorption transitions within the manifold of $v' = 4 \leftarrow v'' = 5$. The mole fraction of NO would be determined as before but now more precisely with use of the measured temperature.

Positioned at 226.073 nm, the laser wavelength also promotes O_2 transitions within the absorption manifolds of $v' = 7 \leftarrow v'' = 6$ and $v' = 13 \leftarrow v'' = 8$, the upper states of which, unlike $v' = 4$, fluoresce primarily at wavelengths shorter than that of the laser. Thus, if oxygen's fluorescence from $190 - 220$ nm were collected as yet a third region, its signal when ratioed against that from region 2 would provide a measure of the vibrational temperature in a manner independent of the local mole fraction of oxygen, a quantity now resolvable from this temperature measurement and either of the two signals that compose it; the mole fraction of NO follows as before. For the excitation wavelength of 226.073 nm in particular, the ratio between regions 3 and 2 as defined would increase by 50% over the temperature range $1800 - 2200$ K. Though promising, this '3-zone' approach is limited in application realistically to cases where the medium is of small enough dimension to appear optically thin at the wavelengths captured by region 3, where high-temperature O_2 presents a strong absorption coefficient (through its $B \leftarrow X$ system).

PARAMETRIC RELATIONS

For the sole purpose of imaging NO as present within fuel-lean high-pressure combustion environments, not every situation will warrant use of the 2-zone technique. especially if the conditions were such that the excitation of NO at any of the five candidate peaks labeled in Figure 1 yielded a favourably large signal ratio of NO to O_2 in region 1. To help the reader gauge the conditions in this regard and also to quantify the dependence of the fluorescence signals on temperature and pressure, we provide coefficients and formulae of empirical, parametric fits to our model's calculation of *i*) the absorption coefficient at the peak of each NO feature labeled in Fig. 1, *ii*) the location in frequency of each peak, and *iii*) the ratio of NO to O_2 fluorescence in region 1 (a tophat bandpass from 230–290 nm).

Each parametric expression is valid in temperature from 1800 – 2200 K, in pressure from 1 – 10 atm, and derives from a least-squares fit to the 20 points resulting from a calculational grid of (1800, 1900, 2000, 2100, 2200 K) by (1, 2, 5, 10 atm). Invariants in the calculations were the spectral distribution of the laser, assumed Gaussian with a FWHM of 0.5 cm^{-1}, and the gas composition of 10 ppm NO, 63% N_2, 10% O_2, 9% CO_2, and 18% H_2O. This distribution of major products of fuel-lean hydrocarbon combustion is an arbitrary compromise between those resulting with air as the oxidizer, where for a stoichiometry of $\phi = 0.5$, for example, the products $N_2/O_2/CO_2/H_2O$ occur in the nominal percentages 75%/10%/6%/9% and those producible in settings, such as a laboratory, where the reactants N_2, O_2 and fuel are of variable proportion. Nonetheless, the parametric fits as developed for the specified product distribution can be scaled quite easily for use with others. The calculated signal ratio of NO to O_2, for example, would be multiplied by the factors $(0.1/X_{O_2})$ and $(X_{NO}/10^{-5})$ if the mole fractions of $O_2(X_{O_2})$ and NO (X_{NO}) were known or suspected to be other than 10% and 10 ppm, respectively. If the percentages of the major constituents differed significantly from those assumed here, the calculated signal ratio could be adjusted for what would amount to a different quenching rate of NO through the multiplicative factor

$$R_Q = \frac{\sum X_a (1 + m_{NO}/m_a)^{0.5} \sigma_a}{\sum X_i (1 + m_{NO}/m_i)^{0.5} \sigma_i},$$

where X_j, m_j, and σ_j are, respectively, the mole fraction, molecular mass, and quenching cross section for species j. The numerator of R_Q pertains to

the assumed (a) product distribution and the denominator to the one of interest (i). Between 1800–2200 K, the quenching cross sections for NO-$A(v=0)$ in collisions with N_2, O_2, CO_2, and H_2O, are essentially constants and may be assigned the respective values 0.7 Å^2, 25 Å^2, 56 Å^2, and 29 Å^2 (Paul et al., 1995; Paul et al., 1993). Also across this span of temperature, the coefficients of collision broadening and collision shift (Chang et al., 1992; Di Rosa and Hanson, 1994a) of the $A \leftarrow X(0,0)$ transitions of NO are sufficiently similar for perturbers N_2, O_2, H_2O, and, very likely, CO_2, that the peak absorption coefficients and frequencies calculated for the candidate features will be reliable without correction for product distributions even very different from the one assumed.

Across the stated calculational grid, the peak absorption coefficient k_{peak} (as convolved with the assumed spectral distribution of the laser) of each candidate feature is recovered to within $\pm 3\%$ by the expression

$$k_{peak} [\mathrm{cm}^{-1}\mathrm{atm}^{-1}] = k_1 / [\ln(P + k_2)]^{k_3} \times e^{(-k_4/T)}/T^2, \qquad (7)$$

where P is the pressure in atmospheres, and T is the temperature in kelvin. For each feature, labeled a through e in Figure 1, Table I lists the fit parameters k_i as well as the dominant features composing each peak. An example of the parametric fit expressed by Eq. (7) is shown in Figure 13 by its match to the absorption coefficient calculated for peak d along the isobars 1, 2, 5, and 10 atm. The positional frequency of each peak, which shifts with temperature and pressure, is fit by

$$v_{peak} [\mathrm{cm}^{-1}] = v^* - f_1 [P^{f_2}(2000/T)^{0.56} - 1], \qquad (8)$$

with v^* designating the feature's peak frequency at 2000 K and 1 atm and the remainder of the expression constituting its shift from this reference position. With the parameters listed in Table I, Eq. (8) fits the calculated peak frequencies to within ± 0.03 cm^{-1}. While the collision-induced shift of individual transitions is directly proportional to pressure for the conditions of interest here, the shift of a peak in the over all absorption spectrum can scale nonlinearly with pressure as the constituent lines blend among themselves and neighbouring transitions.

In the limit of 'linear fluorescence', the number of fluorescence photons N_{peak}^{fl} emitted into 4π steradians can be estimated from Eq. (7), combined with the calculable quenching rate of the $A(v'=0)$ state of NO [6,9],

M. D. Di ROSA *et al.*

TABLE I

Fit parameters for the candidate NO peaks.

Peak	Major Transitions	v^*	Shift		k_1	Peak Abs. Coeff.		k_4	R_1	NO/O$_2$ Ratio		
			f_1	f_2		k_2	k_3			R_2	R_3	R_4
a	$Q_1+P_{21}(15), R_2(16)$	44248.81	0.123	0.672	$1.145(10^8)$	5.145	1.989	117.9	0.2068	2.501	4.570	$1.036(10^4)$
b	$Q_1+P_{21}(14), Q_2+R_{12}(21)$	44241.17	0.157	0.705	$6.221(10^8)$	10.60	3.038	168.6	0.0230	2.257	3.418	$1.353(10^4)$
c	$R_1+Q_{21}(7), P_2+Q_{12}(28)$	44236.49	0.0554	1.06	$1.616(10^8)$	5.069	2.276	589.8	0.2303	2.170	4.676	$1.119(10^4)$
d	$Q_1+P_{21}(13), R_2(15)$	44234.13	0.0579	1.05	$1.139(10^8)$	4.585	2.072	-4.567	1.443	2.817	5.420	$9.936(10^3)$
e	$Q_1+P_{21}(12), Q_2+R_{12}(20)$	44227.66	0.0657	0.967	$5.800(10^8)$	6.287	3.220	328.9	0.9742	3.131	6.216	$1.009(10^4)$
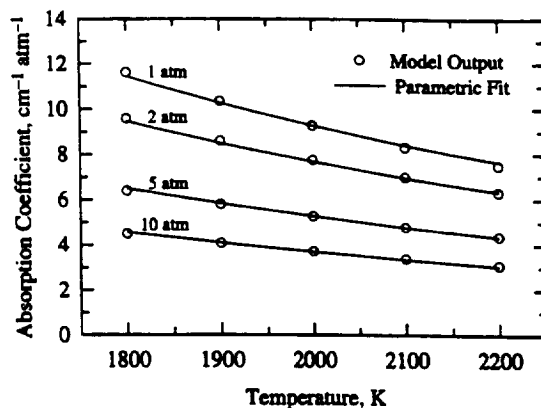
FIGURE 13   Discrete, calculated values of the spectrally-integrated absorption coefficient of peak d compared with the parametric fit provided by Eq. (7) and Table I.

through

$$N_{peak}^{fl} = \frac{k_{peak} P X_{NO}(\Delta \ell) E_0(\Delta V)}{2.0 \times 10^{-23} \times v_{peak}} \times \left[\sum_j A_{0 \to j} \bigg/ Q_{elec} \right], \tag{9}$$

where $\Delta \ell$ [cm] is the pathlength of the laser beam (of local energy density E_0) through the volume ΔV over which the fluorescence is collected. Given by the last term, the quantum efficiency of fluorescence assumes, as appropriate for combustion environments, that Q_{elec} greatly exceeds the total spontaneous emission rate. The summation over the $A_{0 \to j}$ can be restricted, of course, to those vibronic bands encompassed by a particular spectral bandpass. Because the cross sections for quenching are weak functions of temperature between $1800 - 2200$ K, and because $Q_{elec} \propto P$, Eqs. (7) and (9) then relate the temperature- and pressure-dependence of the fluorescence signal of the candidate peaks of NO as simply $k_{peak}(P, T) \times T^{0.5}$.

From $1800 - 2200$ K and $1 - 10$ atm, the calculated ration (R^{fl}) of NO to O_2 fluorescence in region 1 is given to within $\pm 6\%$ by

$$R^{fl} = R_1 / [\ln(P + R_2)]^{R_3} \times e^{(R_4/T)}. \tag{10}$$

As with Eqs. (7) and (8), Eq. (10) pertains to peaks a through e labeled in Figure 1, with the appropriate fitting parameters (the R_i) found in Table I.

The calculations present an upperbound of the fluorescence ratio since, as discussed in connections with Figures 3 and 4, the model for O_2 cannot reasonably include the abosrption transitions from high-lying rotational states, greater than $N'' = 45$, that are beyond the current data base and contribute to the fluorescence signal toward high temperatures. Also, a realistic spectral bandpass will not appear as the tophat assumed for the calculation of R^{fl}. Still, Eq. (10) should provide a fair estimate, within a factor of two, of the relative amounts of NO and O_2 fluorescence within a broad collection bandpass that resides within the $A(v' = 0) \rightarrow X$ bands of NO.

The many combinations of temperature, pressure, and gas composition that might constitute an imaged environment prevent the singular recommendation of a candidate feature, and the foregoing relations are therefore offered to assist the reader's decision. However, of the five candidate features, peak d is calculated to afford the greatest R^{fl} over the range of conditions considered. Figure 14 displays the parametric fit (and, for comparison, the discrete points of the model output) of R^{fl} for peak d, primarily to illustrate expected trends of the NO-to-O_2 signal ratio for flame environments. The noticeably swift degradation of R^{fl} with increasing pressure is typical to the excitation of any peak of NO, a generalization easily reached by examining the distinct trends of the individual signals. As mentioned in connection with Eq. (9), the LIF signal of NO depends on pressure solely through the absorption coefficient, which for a given peak of NO (as excited by a laser of spectral width $\sim 0.5\,\mathrm{cm}^{-1}$) is reduced through collisional broadening by a factor of 2–3 as the pressure increases from 1 to 10 atm.
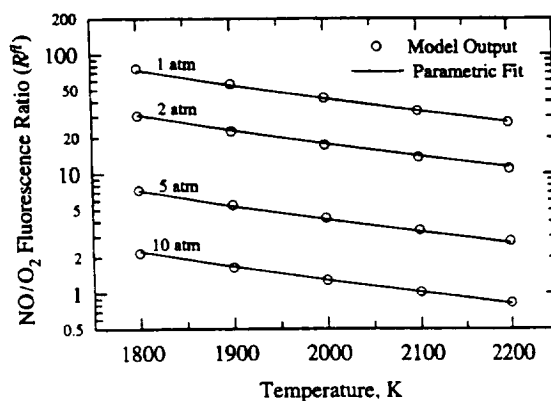
FIGURE 14   NO-to-O_2 fluorescence ratio (R^{fl}) for peak d as calculated by the LIF model and expressed through the parametric fit provided by Eq. (10) and Table I.

The LIF signal from O_2 displays the opposite trend and increases roughly linearly with pressure up to 10 atm because the predissociation rate of the B-state of O_2 prevails over collisional influences in the controlling parameters of absorption coefficient and quantum efficiency of fluorescence. These opposing trends indeed combine for 75% of the total reduction from 1 to 10 atm of the R^{fl} of peak d plotted in Figure 14. The remainder is owed to the change in the absorption coefficient of O_2, which, local to peak d, grows with increasing pressure as collision broadening extends neighbouring transitions into the minimum that underlies peaks a through e. From $1800 - 2200$ K, R^{fl} for each candidate feature falls by about 65% independent of the pressure, owed largely to a diminishing Boltzmann fraction of the absorbing states of NO compounded by a sharp increases in population of the absorbing states of O_2, resident as they are with upper vibrational levels.

CONCLUSIONS

New models of the absorption, excitation, and fluorescence spectra for laser excitations of the $\gamma(0,0)$ band of NO and the Schumann-Runge $(B-X)$ bands of O_2 at high temperatures and pressures were developed and shown, by their comparison with measurements, to have good predictive capabilities for conditions extending to 2000 K and 10 atm. Motivating their development was the application of PLIF imaging of NO as formed in lean, high-pressure combustion environments, conditions under which O_2 can present a troublesome photolytic interference for one-photon excitations within the γ-band of NO.

Identified for excitation were five strong features of the $\gamma(0,0)$ band of NO that lay within a broad minimum in the $B \leftarrow X$ spectrum of O_2, a coincidence necessary for suppressing the interference from O_2 and minimizing the absorptive loss of the laser beam. The advantage in NO signal enjoyed for excitations of these features at moderate temperatures and pressures quickly succumbs, however, to the interference from O_2 as the temperature and pressure increase. At such point, and as illuminated by our models, a strategy of spectrally dividing into two regions the fluorescence induced by a single excitation wavelength may restore to PLIF the capability of measuring NO mole fractions with a sensitivity otherwise possible in the absence of the O_2 interference. Further partitioning the fluorescence distribution might, in certain cases, allow for simultaneous measurements of NO concentration, O_2 concentration, and O_2 vibrational temperature. Fu-

ture work should include an experimental validation of the 2-zone method followed by its application to the PLIF imaging and measurement of the NO concentration generated by high-pressure, lean combustion. Additional data for the B-X bands of O_2—particularly regarding line positions originating with $N'' > 45$, collisional broadening and shift, and processes of energy transfer within and quenching of the B-state—will be required if the models are to be exercised as effectively for conditions exceeding 2000 K and 10 atm.

Acknowledgments

References

Allen, M. G., McManus, K. R. and Sonnenfroh, D. M. (1995) "PLIF Imaging in Spray Flame Combustors at Elevated Pressure," in *Technical Digest of the 33rd Aerospace Sciences Meeting*, American Institute of Aeronautics and Astronautics, Washington, D.C., Paper 95–0172.

Battles, B. E. and Hanson, R. K. (1995) "Laser-Induced Fluorescence Measurements of NO and OH Mole Fraction in Fuel-Lean, High-Pressure (1 – 10 atm) Methane Flames: Fluorescence Modeling and Experimental Validation," *J. Quant. Spectrosc. Radiat. Transfer*, **54**, 521–537.

Battles, B. E., Seitzman, J. M. and Hanson, R. K. (1994) "Quantitative Planar Laser-Induced Fluorescence Imaging of Radical Species in High Pressure Flames," in *Technical Digest of the 32nd Aerospace Sciences Meeting*, American Institute of Aeronautics and Astronautics, Washington, D.C., paper 94–0229.

Bradley, D. and Matthews, K. J. (1968) "Measurement of High Gas Temperatures with Fine Wire Thermocouples," *J. Mech. Eng. Sci.*, **10**, 299–305.

Breene, R. G., Jr.(1961) *The Shift and Shape of Spectral Lines*, Pergamon, New York.

Chang, A. Y., Di Rosa, M. D. and Hanson, R. K. (1992) "Temperature Dependence of Collision Broadening and Shift in the NO A-X(0,0) Band in the Presence of Argon and Nitrogen," *J. Quant. Spectrosc. Radiat. Transfer*, **47**, 375–390.

Creek, D. M. and Nicholls, R. W. (1975) "A Comprehensive Re-Analysis of the O_2 ($B^3\Sigma_u^- - X^3\Sigma_g^-$) Schumann-Runge System," *Proc. R. Soc. Lond. A.*, **341** 517–536.

Di Rosa, M. D. (1996). "High Resolution Line Shape Spectroscopy of Transitions in the Gamma Bands of Nitric Oxide," Ph. D. dissertation, Stanford University, Stanford, CA.

Di Rosa, M. D. and Hanson, R. K. (1994a) "Collision Broadening and Shift of NO γ(0,0) Absorption Lines by O_2 and H_2O at High Temperatures," *J. Quant. Spectrosc. Radiat. Transfer*, **52**, 515–529.

Di Rosa, M. D. and Hanson, R. K. (1994b) "Collision-Broadening and -Shift of NO γ(0,0) Absorption Lines by H_2O, O_2, and NO at 295 K," *J. Molec. Spectrosc.*, **164**, 97–117.

Drayson, S. R. (1976). "Rapid Computation of the Voigt Profile," *J. Quant. Spectrosc. Radiat. Transfer*, **16**, 611–614.

Earls, L. T. (1935) "Intensities in $^2\Pi - {}^2\Sigma$ Transitions in Diatomic Molecules," *Phys. Rev.*, **48**, 423–424.

Engleman, R., Jr. and Rouse, P. E. (1971) "The β and γ Bands of Nitric Oxide Observed During the Flash Photolysis of Nitrosyl Chloride." *J. Molec. Spectrosc.*, **37**, 240–251.

Engleman, R., Jr., Rouse, P. E., Peek, H. M. and Balamonte, V. D. (1970) "Beta and Gamma Band Systems of Nitric Oxide," LA-4364 UC-34 Physics TID-4500, Los Alamos Scientific Laboratory, Los Alamos, NM.

59

Fang, T. -M., Wofsy, S. C. and Dalgarno, A. (1974) "Opacity Distribution Functions and Absorption in Schumann-Runge Bands of Molecular Oxygen," *Planet. Space Sci.,* **22** 413–425.

Gies, H. P. F., Gibson, S. T., McCoy, D. G., Blake, A. J. and Lewis, B. R. (1981) "Experimentally Determined Oscillator Strengths and Linewidths for the Schumann-Runge Band System of Molecular Oxygen–III. The (7 – 0) to (19 – 0) Bands," *J. Quant. Spectrosc. Radiat. Transfer,* **26** 469–481.

Hanson, R. K., Seitzman, J. M. and Paul, P. H. (1990) "Planar Laser-Fluorescence Imaging of Combustion Gases," *Appl. Phys. B.,* **B50**, 441–454.

Hilborn, R. C. (1982) "Einstein Coefficients, Cross Sections, ƒ Values, Dipole Moments, and All That," *Am. J. Phys.,* **50**, 982–986.

Laux, C. O. and Kruger, C. H. (1992) "Arrays of Radiative Transition Probabilities for the N_2 First and Second Positive, NO Beta and Gamma, N_2^+ First Negative, and O_2 Schumann-Runge Band Systems," *J. Quant. Spectrosc. Radiat. Transfer,* **48** 9–24.

Lee, M. P. and Hanson, R. K. (1986) "Calculations of O_2 Absorption and Fluorescence at Elevated Temperatures for Broadband Argon-Fluoride Laser Source at 193 nm," *J. Quant. Spectrosc. Radiat. Transfer,* **36**, 425–440.

Lewis, B. R., Berzins, L., Dedman, C. J. Scholz, T. T. and Carver, J. H. (1988) "Pressure Broadening in the Schumann-Runge Bands of Molecular Oxygen," *J. Quant. Spectrosc. Radiat. Transfer,* **39**, 271–282.

Lewis, B. R., Gibson, S. T. and Dooley, P. M. (1994) "Fine-Structure of Predissociation Linewidth in the Schumann-Runge Bands of Molecular Oxygen," *J. Chem. Phys.,* **100**, 7012–7035.

Locke, R. J., Hicks, Y. R., Anderson, R. C., Ockunzzi, K. A. and North, G. L. (1995) "Two-Dimensional Imaging of OH in a Lean Burning High Pressure Combustor," NASA Technical Memorandum 106854, NASA-Lewis Research Center, Cleveland, OH.

Mallard, W. G., Miller, J. H. and Smyth, K. C. (1982). "Resonantly Enhanced Two-Photon Photoionization of NO in an Atmospheric Flame," *J. Chem. Phys.,* **76**, 3483–3492.

McMillin, B. K., Palmer, J. L. and Hanson, R. K. (1993) "Temporally Resolved, Two-Line Fluorescence Imaging of NO Temperature in a Transverse Jet in a Supersonic Cross Flow," *Appl. Opt.,* **32** 7532–7545.

Miller, S. L. and Townes, C. H. (1953) "The Microwave Absorption Spectrum of $(O^{16})_2$ and $O^{16}O^{17}$," *Phys. Rev.,* **90**, 537–541.

Nicolet, M. N., Cieslik, S. and Kennes, R. (1989) "Aeronomic Problems of Molecular Oxygen Photodissociation–V. Predissociation in the Schumann-Runge Bands of Oxygen," *Planet. Space Sci.,* **37**, 427–458.

Paul, P. H., Carter, C. D., Gray, J. A., Durant, J. L. J., Thoman, J. W. and Furlanetto, M. R. (1995) "Correlations for the NO $A^2\Sigma^+(v' = 0)$ Electronic Quenching Cross-Section," Sandia Report SAND94-8237UC-1423, Sandia National Laboratories, Livermore, CA.

Paul, P. H., Gray, J. A., Durant, J. L. J. and Thoman, J. W. J. (1993) "A Model for Temperature-Dependent Collisional Quenching of NO $A^2\Sigma^+$," *Appl. Phys.,* B. **B57**, 249–259.

Reisel, J. R., Partidge, W. P., Jr. and Laurendeau, N. M. (1994) "Transportability of a Laser-Induced Fluorescence Calibration for NO at High-Pressure," *J. Quant. Spectrosc. Radiat. Transfer,* **53**, 165–178.

Schiengraber, H. and Vidal, C. R. (1985) "Measurement of Hönl-London Factors on $^2\Sigma^+ - ^2\Pi$ Transitions of NO," *J. Chem. Phys.,* **85**, 3873–3877.

Tatum, J. B. and Watson, J. K. G. (1971) "Rotational Line Strengths in $^3\Sigma^\pm - ^3\Sigma^\pm$ Transitions with Intermediate Coupling," *Can. J. Phys.* **49**, 2693–2703.

Westblom, U., Fernandez-Alonso, F., Mahon, C. R., Smith, G. P., Jeffries, J. B. and Crosley, D. R. (1994) "Laser-Induced Fluorescence Diagnostics of a Propane/Air Flame with a Manganese Fuel Additive," *Combust. Flame,* **99**, 261–268.

Williams, B. A. and Fleming, J. W. (1994). "Comparative Species Concentrations in $CH_4/O_2/Ar$ Flames Doped with N_2O,NO, and NO_2," *Combust. Flame,* **98**, 93–106.

Wysong, I. J., Jeffries, J. B. and Crosley, D. R. (1989) "Laser-Induced Fluorescence of $O(3p^3P)$, O_2, and NO near 226 nm: Photolytic Interferences and Simulatneous Excitation in Flames," *Opt. Lett.,* **14**, 767–769.

Zare, R. N. (1988). *Angular Momentum,* John Wiley and Sons, New York.

SECTION 6.3: NO/O₂ Computer Code

Codes for absorption, excitation, and fluorescence spectra of NO A–X and O_2 B–X are available to assist in the design of absorption-based or LIF-based experiments. The use of each code (six total, 3 apiece for NO and O_2) should be self-explanatory from the annotated input file, and so only general features are listed here. Overviews and sample output from the codes, and the literature they draw upon, are available from M. D. Di Rosa, K. G. Klavuhn, and R. K. Hanson, *Combustion Science and Technology*, vol. 118, pp. 257-283 (1996) and M. D. Di Rosa, *High-Resolution Line Shape Spectroscopy of Transitions in the Gamma Bands of Nitric Oxide*, Topical Report T-327, Mechanical Engineering Department, Thermosciences Division, Stanford University, Stanford CA (1996). The codes are offered without assistance from the aforementioned authors in their compilation, use, and interpretation.

Absorption [NO A←X(0,0), O₂ B←X]
- Returns the absorption spectrum in units of cm^{-1} atm^{-1} (right column) versus cm^{-1} (left column) for the specified conditions and wavelength range.
- Accommodates Gaussian laser width
- Calculates collision broadening for a given mixture.
- Lists all transitions composing the absorption spectrum.

Excitation [NO A←X(0,0), O₂ B←X]
- Returns the excitation spectrum versus cm^{-1} (left column) in units (right column) of total fluorescence photons through the spectral bandpass and emitted into 4π sr per mJ of laser energy, per mm of path length, and per unit partial pressure of the absorber.
- Accommodates Gaussian laser width
- Accounts for collision broadening and electronic quenching.
- Provides bandpass filters of common PMT/Schott Glass combinations. Allows user-specified bandpasses as well.
- Calculates NO spectra in specified limit of zero or complete RET in NO–A(v=0).

Fluorescence [NO A(v=0)→X, O₂ B→X]
- Returns the fluorescence spectrum versus cm^{-1} (left column) for a specified excitation wavelength in units (right column) of total fluorescence photons through a specified instrument width and emitted into 4π sr per mJ of laser energy, per mm of path length, and per unit partial pressure of the absorber.
- Accommodates Gaussian laser width and arbitrary instrument width (*i.e.*, spectrometer resolution).
- Lists all transitions overlapped with the excitation frequency.
- Accounts for collision broadening and electronic quenching.
- Calculates NO spectra in specified limit of zero or complete RET in NO–A(v=0).

Limits
- NO spectra: $T \leq 2500$ K, $\rho \leq 5$ Amagat (1 Amagat = 2.7×10^{19} cm^{-3})

- O_2 spectra: T $\leq$ 2000 K, P $\leq$ 10 atm

Source Files and Compilation

Codes for the absorption, excitation, and fluorescence spectra are compiled separately for NO and O_2. All are written in Fortran 77 and have been compiled successfully on a Dec Alpha (with an f90 compiler) and Microsoft Fortran PowerStation 4.0. Each is constructed similarly, with a driver (.f extension) that accesses common routines in a main program (??main.f) that, in turn, retrieves spectroscopic parameters from several 'include' files (.lb suffix). Input files have an .inp suffix.

NO Codes: Common to all are the main source program (nomain.f), the line-shape function voigt.f, and the 'include' files A_ul_no.lb, no-A_state.lb, no-X_state.lb, and noA-Xengl.lb. Absorption, excitation, and fluorescence codes require the following pairs of [driver/input] files: Absorption [noabs.f/in_noabs.inp]; Excitation [noexcit.f/in_noex.inp]; Fluorescence [nofluor.f/in_nofl.inp].

O2 Codes: Common to all are the main source program (o2main.f), the line-shape function voigt.f, and the 'include' files o2_X_spec.lb, o2_B_spec.lb, o2_BtoX_EinA.lb, and lewis.lb. Absorption, excitation, and fluorescence codes require the following pairs of [driver/input] files: Absorption [o2b-xabs.f/in_o2abs.inp]; Excitation [o2excit.f/in_o2ex.inp]; Fluorescence [o2fluor.f/in_o2fl.inp].

Instructions for Downloading via ftp

1. connect via ftp to navier.stanford.edu

2. login: anonymous; password: guest

3. cd /pub/spectra

4. retrieve routines of interest